

Phonon affected transport through molecular quantum dots

J Loos[†], T Koch[‡], A Alvermann[‡], A R Bishop[§], and H Fehske[‡]

[†] Institute of Physics, Academy of Sciences of the Czech Republic, 16200 Prague, Czech Republic

[‡] Institute of Physics, Ernst-Moritz-Arndt University Greifswald, 17487 Greifswald, Germany

[§] Theory, Simulation and Computation Directorate, Los Alamos National Laboratory, Los Alamos, New Mexico 87545, USA

E-mail: loos@fzu.cz

Abstract. To describe the interaction of molecular vibrations with electrons at a quantum dot contacted to metallic leads, we extend an analytical approach that we previously developed for the many-polaron problem. Our scheme is based on an incomplete variational Lang-Firsov transformation, combined with a perturbative calculation of the electron-phonon self-energy in the framework of generalised Matsubara functions. This allows to describe the system at weak to strong coupling and intermediate to large phonon frequencies. We present results for the quantum dot spectral function and for the kinetic coefficient that characterises the electron transport through the dot. With these results we critically examine the strengths and limitations of our approach, and discuss the properties of the molecular quantum dot in the context of polaron physics. We place particular emphasis on the importance of corrections to the concept of an antiadiabatic dot polaron suggested by the complete Lang-Firsov transformation.

PACS numbers: 73.63.Kv, 71.38.-k, 73.21.La, 72.10.-d

Submitted to: *J. Phys.: Condens. Matter*

1. Introduction

Recent advances in nanotechnology have stimulated great interest in the basic mechanisms of transport through molecular junctions (Chen et al. 1990, Park et al. 2002, Reichert et al. 2002, Kubatkin et al. 2003, Park 2007, Cuniberti et al. 2005). In such devices the central element can be a single organic molecule, but also a suspended carbon nanotube, which may be thought of as a quantum dot contacted to metallic leads that act as macroscopic charge reservoirs. Transport through a quantum dot is determined by energy level quantisation as well as electron correlation and electron-phonon (EP) interaction effects (Alexandrov & Bratkovsky 2003, Mitra et al. 2004, Takei et al. 2005, Galperin et al. 2007, Fehske et al. 2008).

Vibrations of a molecular quantum dot are local excitations of substantial energy, which are represented by optical phonons. Their frequency is comparable to the transfer integral or kinetic energy of electrons (Nuñez Regueiro et al. 2007). Therefore, the mobility of electrons is significantly modified by the influence of molecular vibrations. In this respect, a molecular quantum dot resembles the situation in a crystalline structure, where the coupling between vibrations and electrons may lead to the formation of (small) polarons, as studied in the context of Holstein's molecular crystal model (Holstein 1959*a*, Holstein 1959*b*). A Holstein polaron is an electron dressed by an accompanying phonon cloud. Since the polaron must carry the deformation through the lattice, the mobility of Holstein polarons can be lowered by several orders of magnitude in comparison to the free electronic excitation (Lang & Firsov 1962). While the physics of Holstein polarons in a perfect crystal at low temperature and small density is by now well understood (see e.g. the review (Fehske & Trugman 2007)), there is less understanding if the periodicity of the crystal is altered, e.g. by impurities (Mishchenko et al. 2009, Alvermann & Fehske 2008) or disorder (Bronold & Fehske 2002, Bronold et al. 2004), in anisotropic materials (Alvermann et al. 2008, Emin 1986), or is absent for complicated geometries.

For a molecular quantum dot, translational symmetry is broken from the outset, and EP coupling is relevant only in a small part of the entire system. The electron current through a deformable quantum dot was found to depend significantly on the local EP coupling (Flensberg 2003, Nuñez Regueiro et al. 2007, Zazunov & Martin 2007, Mitra et al. 2004, Takei et al. 2005, Hohenadler & Fehske 2007). In order to understand the basic transport mechanisms in such devices, appropriate theoretical models have to be studied. The most simple model corresponds to a modified Fano-Anderson model, where a vibrating quantum dot replaces the static impurity. Then the current is determined by a dot spectral function (Meir & Wingreen 1992). The spectral function contains the influence of the leads, as well as the renormalisation by EP coupling. In particular, it determines the charge carrier population of the dot, and its value close to the Fermi energy of the leads determines the number of electrons contributing to the current. Since, with increasing EP interaction, spectral weight is transferred to lower energies, the charge carrier population of the dot increases. For the current, on the other hand, a reduction is expected since the spectral weight at the Fermi energy decreases.

In the present manuscript we will address electron transport through a deformable molecule within an approximate description, which we previously developed for Holstein polarons at finite density (Loos, Hohenadler & Fehske 2006, Loos, Hohenadler, Alvermann & Fehske 2006, Loos et al. 2007). It accounts for renormalisation and inelastic processes, and Pauli blocking. Higher order many-particle processes, namely the further excitation of electron-hole pairs and subsequent evolution of many-particle correlations, are not included. The current presentation, therefore, should be considered as an important but intermediate step towards a complete description. A particular feature of our approach is that it interpolates between weak and strong coupling using an incomplete variational Lang-Firsov transformation. As a consequence it describes

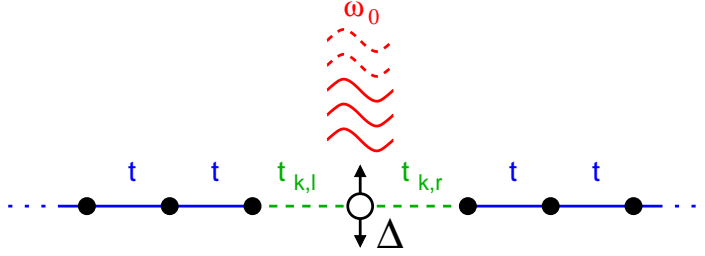


Figure 1. (Colour online) Sketch of a molecular quantum dot with vibrational frequency ω_0 between two metallic leads.

polaronic effects without being restricted to the antiadiabatic strong coupling regime. We introduce our approach here for the current treated in linear response, where the kinetic coefficient is obtained from the dot spectral function at equilibrium. Subsequent work will address the current at finite voltage bias.

The paper is organised as follows. In section 2.1 we introduce the model Hamiltonian, and describe the variational Lang-Firsov transformation. In section 2.2 we derive the expressions and the iterative calculation scheme for the self-energy, which depends on the variational parameter of the incomplete Lang-Firsov transformation. This parameter is obtained from minimisation of the energy, which we express as the expectation value of the Hamiltonian within the approximation used. From the spectral function, the kinetic coefficient is obtained in section 2.4. section 3 discusses the numerical results, and we conclude in section 4.

2. Theoretical Approach

2.1. Model

The paradigmatic example of a vibrating quantum dot is provided by a molecule sandwiched between two metallic leads (see figure 1). Such a system can be described by the Hamiltonian

$$H = \sum_{k,a} \xi_{ka} c_{ka}^\dagger c_{ka} - \frac{1}{\sqrt{N}} \sum_{k,a} \left(t_{ka} d^\dagger c_{ka} + t_{ka}^* c_{ka}^\dagger d \right) + \eta d^\dagger d - g\omega_0 (b^\dagger + b) d^\dagger d + \omega_0 b^\dagger b \quad (1)$$

with $\xi_{ka} = E_{ka} - \mu_a$, $\mu = \frac{1}{2}(\mu_l + \mu_r)$, and $\eta = \Delta - \mu$. Here, the E_{ka} (for $k = 1, \dots, N$) give the energies of non-interacting electrons in the left and right lead $a = l, r$, and c_{ka}^\dagger (c_{ka}) are the corresponding creation (destruction) operators of free fermions in the N lead states. The population of the leads is determined by the chemical potentials μ_a . The quantum dot is represented by a single energy level Δ , with Fermi operators $d^{(\dagger)}$. The term $\propto t$ ($\propto t^*$) allows for lead-dot (dot-lead) particle transfer. An electron at the quantum dot interacts via a Holstein-type coupling with a local (intra-molecular) vibrational mode; g denotes the dimensionless EP coupling constant, and ω_0 the frequency of the optical phonons created (annihilated) by b^\dagger (b).

The quantum dot responds to the presence of an electron with a finite deformation. For sufficiently large phonon frequency ω_0 , the strength of the deformation depends only on the momentary occupancy of the dot. This is in analogy to Holstein's small polaron theory, where a lattice deformation in the vicinity of the electron accompanies the electron motion. To describe this effect, we apply a generalised Lang-Firsov displacement transformation (Lang & Firsov 1962) with parameter $\gamma \in [0, 1]$,

$$U = e^{\tilde{g}(b^\dagger - b)d^\dagger d}, \quad \text{for} \quad \tilde{g} = \gamma g. \quad (2)$$

After this transformation, the original electron and phonon operators are given as

$$\tilde{d} = e^{\tilde{g}(b^\dagger - b)} d, \quad \tilde{b} = b + \tilde{g} d^\dagger d. \quad (3)$$

The transformed Hamiltonian $\tilde{H} = U^\dagger H U$ reads

$$\begin{aligned} \tilde{H} = & \sum_{k,a} \xi_{ka} c_{ka}^\dagger c_{ka} - \sum_{k,a} \left(C_{ka} d^\dagger c_{ka} + C_{ka}^\dagger c_{ka}^\dagger d \right) \\ & + \tilde{\eta} d^\dagger d - C_d d^\dagger d + \omega_0 b^\dagger b, \end{aligned} \quad (4)$$

where

$$C_{ka} = \frac{1}{\sqrt{N}} t_{ka} e^{-\tilde{g}(b^\dagger - b)}, \quad C_d = g\omega_0(1 - \gamma)(b^\dagger + b), \quad (5)$$

and

$$\tilde{\eta} = \Delta - \mu - \varepsilon_p \gamma (2 - \gamma), \quad \text{with} \quad \varepsilon_p = g^2 \omega_0. \quad (6)$$

As the parameter γ of the Lang-Firsov transformation grows from $\gamma = 0$ to $\gamma = 1$ it accounts for the transition between the weak-coupling and strong-coupling regimes. The value of γ will be later determined from minimisation of the energy. Only for very strong coupling and large phonon frequency, is the value $\gamma = 1$ approached. Then, the canonical transformation (2) eliminates the direct coupling term between the new fermion and shifted boson operators at the price of introducing a boson modified transfer term between quantum dot and leads. This corresponds to the strong-coupling limit of polaron theory, where the new Fermi operators d would represent small polarons in the deformable lattice. For our problem, 'polaron formation' at the quantum dot mainly results in lowering of the dot energy level by the polaron shift ε_p , and in an exponential reduction of the effective dot-lead transfer $\tilde{t}_{ka} = t_{ka} e^{-\tilde{g}^2/2}$. Note that the variation of γ throughout the parameter regime is important to describe the system away from the strong-coupling limit. The use of the γ -dependent variational Lang-Firsov transformation is an essential feature of our description.

2.2. Single-particle properties: quantum-dot spectral function

We first determine the retarded Green function G_{dd} of the quantum dot, which is represented by the operators $d^{(\dagger)}$ in the transformed Hamiltonian (4). The Green function is calculated within perturbation theory up to second order in the interaction coefficients (5), starting from the Lang-Firsov transformed Hamiltonian (4). Since the parameter γ is assigned variationally, this treatment exceeds standard weak-coupling

or strong-coupling perturbation theory, which starts either from the untransformed Hamiltonian (corresponding to $\gamma = 0$) or the fully transformed Hamiltonian ($\gamma = 1$). The combination of perturbation theory with an incomplete variational Lang-Firsov transformation provides meaningful results also away from these limiting cases.

Our calculation is based on the equations of motion for the generalised temperature Green functions (Kadanoff & Baym 1962), adapted to systems with EP interaction (Bruevich & Tyablikov 1962, Schnakenberg 1966). Accordingly we define

$$G_{dd}(\tau_1, \tau_2; \{V\}) = -\frac{1}{\langle S \rangle} \langle \mathcal{T}_\tau d(\tau_1) d^\dagger(\tau_2) S \rangle, \quad (7)$$

and in an analogous way G_{cd} , G_{dc} , and G_{cc} , with

$$S = \mathcal{T}_\tau \exp \left\{ - \int_0^\beta d\tau H_{int}(\tau) \right\}, \quad (8)$$

$$H_{int}(\tau) = \sum_{k,a} \left(V_{ka}(\tau) C_{ka}(\tau) + \bar{V}_{ka}(\tau) C_{ka}^\dagger(\tau) \right) + V_d(\tau) C_d(\tau), \quad (9)$$

where the classical variables V_{ka} , \bar{V}_{ka} , and V_d were introduced as a purely formal device.

We set up the equations of motion for the Green functions using the following matrix notation

$$\int_0^\beta d\tau' G_1(\tau_1, \tau'; \{V\}) G_2(\tau', \tau_2; \{V\}) \equiv G_1(\tau_1, \tau'; \{V\}) \circ G_2(\tau', \tau_2; \{V\}). \quad (10)$$

If G_1 , G_2 satisfy the relation

$$G_1(\tau_1, \tau'; \{V\}) \circ G_2(\tau', \tau_2; \{V\}) = \delta[\tau_1 - \tau_2], \quad (11)$$

they are called inverse functions of each other. In particular, the inverse functions to the zeroth-order Green functions $G_{dd}^{(0)}(\tau_1, \tau_2)$ and $G_{cc;ka}^{(0)}(\tau_1, \tau_2)$ are given as

$$G_{dd}^{(0)-1}(\tau_1, \tau_2) = \left[-\frac{\partial}{\partial \tau_1} - \tilde{\eta} \right] \delta[\tau_1 - \tau_2] \quad (12)$$

and

$$G_{cc;ka}^{(0)-1}(\tau_1, \tau_2) = \left[-\frac{\partial}{\partial \tau_1} - \xi_{ka} \right] \delta[\tau_1 - \tau_2], \quad (13)$$

respectively. By functional derivation with respect to the auxiliary fields $\{V\}$ we find a set of coupled equations,

$$\begin{aligned} G_{dd}^{(0)-1}(\tau_1, \tau') \circ G_{dd}(\tau', \tau_2; \{V\}) &= \delta[\tau_1 - \tau_2] \\ &- \bar{C}_d(\tau_1, \{V\}) G_{dd}(\tau_1, \tau_2; \{V\}) + \frac{\delta}{\delta V_d(\tau_1)} G_{dd}(\tau_1, \tau_2; \{V\}) \\ &- \sum_{k,a} \bar{C}_{k,a}(\tau_1, \{V\}) G_{cd;ka}(\tau_1, \tau_2; \{V\}) \\ &+ \sum_{k,a} \frac{\delta}{\delta V_{ka}(\tau_1)} G_{cd;ka}(\tau_1, \tau_2; \{V\}), \end{aligned} \quad (14)$$

$$G_{cc;ka}^{(0)-1}(\tau_1, \tau') \circ G_{cd;ka}(\tau', \tau_2; \{V\}) = -\bar{C}_{ka}^\dagger(\tau_1, \{V\})G_{dd}(\tau_1, \tau_2; \{V\}) + \frac{\delta}{\delta \bar{V}_{ka}(\tau_1)}G_{dd}(\tau_1, \tau_2; \{V\}), \quad (15)$$

with $\bar{C}_d(\tau, \{V\}) = \frac{1}{\langle S \rangle} \langle \mathcal{T}_\tau C_d(\tau) S \rangle$, $\bar{C}_{ka}(\tau, \{V\}) = \frac{1}{\langle S \rangle} \langle \mathcal{T}_\tau C_{ka}(\tau) S \rangle$, and $\bar{C}_{ka}^\dagger(\tau, \{V\}) = \frac{1}{\langle S \rangle} \langle \mathcal{T}_\tau C_{ka}^\dagger(\tau) S \rangle$.

In order to solve this system of equations, we multiply (15) by $G_{cc}^{(0)}$ from the left and substitute the resulting expression for G_{cd} in (14). Then equation (14) is multiplied by G_{dd}^{-1} from the right. The resulting equation for G_{dd} is converted to an equation for the self-energy Σ_{dd} , introduced by

$$G_{dd}^{-1}(\tau_1, \tau_2; \{V\}) = G_{dd}^{(0)-1}(\tau_1, \tau_2) - \Sigma_{dd}(\tau_1, \tau_2; \{V\}). \quad (16)$$

By use of the functional differentiation rules

$$\delta G \circ G^{-1} = -G \circ \delta G^{-1} = G \circ \delta \Sigma, \quad \delta G = G \circ \delta \Sigma \circ G, \quad (17)$$

the self-energy Σ becomes

$$\begin{aligned} \Sigma_{dd}(\tau_1, \tau_2; \{V\}) = & -\bar{C}_d(\tau_1; \{V\})\delta[\tau_1 - \tau_2] \\ & + \sum_{k,a} \bar{C}_{ka}(\tau_1; \{V\})G_{cc;ka}^{(0)}(\tau_1, \tau_2)\bar{C}_{ka}^\dagger(\tau_2; \{V\}) \\ & - \sum_{k,a} G_{cc;ka}^{(0)}(\tau_1, \tau_2) \frac{\delta \bar{C}_{ka}^\dagger(\tau_2; \{V\})}{\delta \bar{V}_{ka}(\tau_1)} + G_{dd}(\tau_1, \tau'; \{V\}) \circ \frac{\delta \Sigma_{dd}(\tau', \tau_2; \{V\})}{\delta \bar{V}_d(\tau_1)} \\ & - \sum_{k,a} \bar{C}_{ka}(\tau_1; \{V\})G_{cc;ka}^{(0)}(\tau_1, \tau'') \circ G_{dd}(\tau'', \tau'; \{V\}) \circ \frac{\delta \Sigma_{dd}(\tau', \tau_2; \{V\})}{\delta \bar{V}_{ka}(\tau'')} \\ & - \sum_{k,a} G_{cc;ka}^{(0)}(\tau_1, \tau'') \bar{C}_{ka}^\dagger(\tau''; \{V\}) \circ G_{dd}(\tau'', \tau'; \{V\}) \circ \frac{\delta \Sigma_{dd}(\tau', \tau_2; \{V\})}{\delta \bar{V}_{ka}(\tau_1)} \\ & + \text{terms with products of functional derivatives of } \Sigma_{dd} \\ & + \text{terms with second functional derivatives of } \Sigma_{dd}. \end{aligned} \quad (18)$$

Within our iterative scheme, the terms on the r.h.s. of equation (18) without functional derivatives of Σ_{dd} are taken in the first step as $\Sigma_{dd}^{(1)}(\tau_1, \tau_2; \{V\})$. Explicitly, we have

$$\begin{aligned} \Sigma_{dd}^{(1)}(\tau_1, \tau_2; \{V\}) = & -\bar{C}_d(\tau_1; \{V\})\delta[\tau_1 - \tau_2] \\ & + \sum_{k,a} \bar{C}_{ka}(\tau_1; \{V\})G_{cc;ka}^{(0)}(\tau_1, \tau_2)\bar{C}_{ka}^\dagger(\tau_2; \{V\}) \\ & + \sum_{k,a} G_{cc;ka}^{(0)}(\tau_1, \tau_2) \left[\frac{1}{\langle S \rangle} \langle \mathcal{T}_\tau C_{ka}(\tau_1) C_{ka}^\dagger(\tau_2) S \rangle - \bar{C}_{ka}(\tau_1; \{V\})\bar{C}_{ka}^\dagger(\tau_2; \{V\}) \right]. \end{aligned} \quad (19)$$

In the second step, to obtain $\Sigma_{dd}^{(2)}$, the first approximation $\Sigma_{dd}^{(1)}$ has to be inserted into the functional derivatives of Σ_{dd} on the r.h.s. of (18). But, if we confine ourselves to terms up to second order in the interaction coefficients, only the first four terms on the

r.h.s. are relevant. In this approximation, the self-energy $\Sigma_{dd}(\tau_1, \tau_2) = \Sigma_{dd}(\tau_1, \tau_2; \{0\})$, determining the temperature Green function $G_{dd}(\tau_1, \tau_2) = G_{dd}(\tau_1, \tau_2; \{0\})$, is given as

$$\Sigma_{dd}(\tau_1, \tau_2) = \Sigma_{dd}^{(1)}(\tau_1, \tau_2; \{0\}) + G_{dd}(\tau_1, \tau_2) \langle \mathcal{T}_\tau C_d(\tau_1) C_d(\tau_2) \rangle, \quad (20)$$

where $\bar{C}_d(\tau; \{0\}) = 0$ and $\bar{C}_{ka}(\tau; \{0\}) = [\bar{C}_{ka}^\dagger(\tau; \{0\})]^* = \frac{1}{\sqrt{N}} t_{ka} \exp\{-\frac{1}{2} \tilde{g}^2 \coth(\frac{1}{2} \beta \omega_0)\}$. The correlation functions of the interaction coefficients occurring in (20) have been calculated in previous work for the generalised Lang-Firsov transformation in the Holstein model (Fehske et al. 1997). Converting (20) to the equation for the Fourier transform of the self-energy and expressing the Fourier transform of G_{dd} , $G_{dd}(i\omega_\nu)$, by means of the spectral function A_{dd} , the summation over the bosonic Matsubara frequencies $\omega_n = 2n\pi/\beta$ (being the difference of two fermionic Matsubara frequencies) can be carried out, and we obtain, within low-temperature approximation ($\beta\omega_0/2 \gg 1$),

$$\begin{aligned} \Sigma_{dd}(i\omega_\nu) = & \frac{1}{N} \sum_{k,a} e^{-\tilde{g}^2} |t_{ka}|^2 \frac{1}{i\omega_\nu - \xi_{ka}} \\ & + \sum_{s \geq 1} e^{-\tilde{g}^2} \frac{(\tilde{g}^2)^s}{s!} \frac{1}{N} \sum_{k,a} |t_{ka}|^2 \left(\frac{n_F(\xi_{ka})}{i\omega_\nu - \xi_{ka} + s\omega_0} + \frac{1 - n_F(\xi_{ka})}{i\omega_\nu - \xi_{ka} - s\omega_0} \right) \\ & + [(1 - \gamma)g\omega_0]^2 \int_{-\infty}^{+\infty} d\omega' A_{dd}(\omega') \left(\frac{n_F(\omega')}{i\omega_\nu - \omega' + \omega_0} + \frac{1 - n_F(\omega')}{i\omega_\nu - \omega' - \omega_0} \right), \end{aligned} \quad (21)$$

with the fermionic Matsubara frequencies $\omega_\nu = (2\nu + 1)\pi/\beta$ and the Fermi function $n_F = (e^{\beta\omega} + 1)^{-1}$. Analytical continuation $i\omega_\nu \rightarrow \bar{\omega} = \omega + i\delta$ in the upper complex half-plane then gives the retarded Green function

$$G_{dd}^R(\bar{\omega}) = \frac{1}{\bar{\omega} - \tilde{\eta} - \Sigma_{dd}(\bar{\omega})} \quad (22)$$

and the related spectral function

$$A_{dd}(\omega) = -\frac{1}{\pi} \text{Im} G_{dd}^R(\omega + i0^+). \quad (23)$$

The r.h.s. of equation (23) is determined by the real and imaginary parts of $\Sigma_{dd}(\omega + i0^+)$, which we obtain from (21) employing $\frac{1}{x+i0^+} = \mathcal{P}\frac{1}{x} - i\pi\delta(x)$. Moreover, we transform the k -summation into an integration over the band energy ξ of the leads, $\xi \in [-W, W]$, using the substitution $dk = g(\xi)d\xi$ and taking into account the evenness of the functions in (21) with respect to k . Assuming further the right and the left leads to be identical the summation over a gives simply a factor 2. In the end, we work in the limit $T \rightarrow 0$, when the Fermi function becomes the Heaviside function, $n_F = \Theta(-\omega)$, and obtain

$$\begin{aligned} \text{Im} \Sigma_{dd}(\omega) = & -2e^{-\tilde{g}^2} |t(\omega + \mu)|^2 g(\omega + \mu) \int_{-W}^W d\xi \delta[\omega - (\xi - \mu)] \\ & - 2e^{-\tilde{g}^2} \sum_{s \geq 1} \frac{(\tilde{g}^2)^s}{s!} \left\{ [g(\xi)|t(\xi)|^2]_{\xi=\omega+\mu+s\omega_0} \int_{-W}^{\mu} d\xi \delta[\omega - (\xi - \mu) + s\omega_0] \right. \\ & + [g(\xi)|t(\xi)|^2]_{\xi=\omega+\mu-s\omega_0} \int_{\mu}^W d\xi \delta[\omega - (\xi - \mu) - s\omega_0] \Big\} \\ & - \pi [(1 - \gamma)g\omega]^2 \{A_{dd}(\omega + \omega_0)\Theta(-\omega - \omega_0) + A_{dd}(\omega - \omega_0)\Theta(\omega - \omega_0)\}, \end{aligned} \quad (24)$$

$$\begin{aligned}
\text{Re } \Sigma_{dd}(\omega) = & e^{-\tilde{g}^2} \frac{2}{\pi} \mathcal{P} \int_{-W}^W d\xi g(\xi) |t(\xi)|^2 \frac{1}{\omega - (\xi - \mu)} \\
& e^{-\tilde{g}^2} \frac{2}{\pi} \sum_{s \geq 1} \frac{(\tilde{g}^2)^s}{s!} \mathcal{P} \left\{ \int_{-W}^{\mu} d\xi g(\xi) |t(\xi)|^2 \frac{1}{\omega - (\xi - \mu) + s\omega_0} \right. \\
& \quad \left. + \int_{\mu}^W d\xi g(\xi) |t(\xi)|^2 \frac{1}{\omega - (\xi - \mu) - s\omega_0} \right\} \\
& + [(1 - \gamma)g\omega_0]^2 \left\{ \mathcal{P} \int_{-\infty}^0 d\omega' \frac{A_{dd}(\omega')}{\omega + \omega_0 - \omega'} + \mathcal{P} \int_0^{\infty} d\omega' \frac{A_{dd}(\omega')}{\omega - \omega_0 - \omega'} \right\}.
\end{aligned} \tag{25}$$

Note that in accordance with our second order approach, the spectral functions $A_{dd}(\omega)$ occurring in (24), (25) have to be determined by equations (22), (23), using $\Sigma_{dd}^{(1)}(\omega + i0^+)$ for the self-energy.

For $g = 0$, we are faced with the well-known problem of electron localisation at an impurity. Then, if a solution $\tilde{\omega}$ of

$$\tilde{\omega} = \Delta + \text{Re } \Sigma_{dd}(\tilde{\omega} - \mu) \tag{26}$$

exists outside the interval $[-W, W]$, the spectral function $A_{dd}(\omega)$ exhibits a single-peak structure,

$$A_{dd}(\omega) = z(\tilde{\omega}) \delta[\omega - (\tilde{\omega} - \mu)], \tag{27}$$

reflecting electron localisation at the quantum dot. Here,

$$z(\tilde{\omega})^{-1} = \left| 1 + \frac{2}{\pi} \mathcal{P} \int_{-W}^W d\xi g(\xi) |t(\xi)|^2 \frac{1}{(\tilde{\omega} - \xi)^2} \right|. \tag{28}$$

According to the first term on the r.h.s. of (24), we find $\text{Im } \Sigma_{dd}(\omega) \neq 0$ for $\omega \in [-W - \mu, W - \mu]$, leading to an incoherent single-particle spectrum in this interval.

For non-zero coupling between the electron and the local vibrational mode at the dot, we have $\text{Im } \Sigma_{dd}(\omega) \neq 0$ everywhere provided that $[-\omega_0, +\omega_0] \subset [-W - \mu, W - \mu]$. Then, if $g \neq 0$, the spectral function $A_{dd}(\omega)$ exhibits no coherent contribution, and is given, for all ω and $\gamma \in [0, 1]$, by a purely incoherent spectrum

$$A_{dd}(\omega) = -\frac{1}{\pi} \frac{\text{Im } \Sigma_{dd}(\omega)}{[\omega - \tilde{\eta} - \text{Re } \Sigma_{dd}(\omega)]^2 + [\text{Im } \Sigma_{dd}(\omega)]^2}. \tag{29}$$

On the other hand, if the latter condition is not fulfilled because either $-\omega_0 < -W - \mu$ or $W - \mu < \omega_0$, then the contributions to $\text{Im } \Sigma_{dd}(\omega)$ from the phonon processes

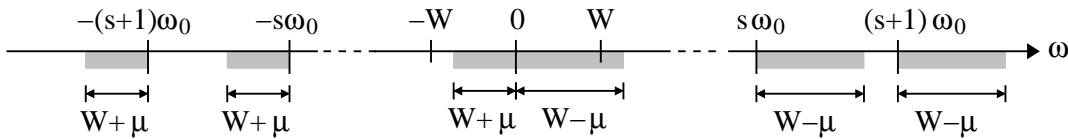


Figure 2. Shaded regions indicate the intervals of non-zero contributions to $\text{Im } \Sigma_{dd}(\omega)$ from the processes determined by the first two terms on the r.h.s. of equation (24). Note that all intervals overlap if $[-\omega_0, \omega_0] \subset [-W - \mu, W - \mu]$. Shown is the case $\omega_0 > W$, $\mu < 0$.

vanish in certain ω -intervals (see figure 2). In particular, this happens for $\omega < 0$, $\omega \in (-(s+1)\omega_0, -s\omega_0 - W - \mu)$ and for $\omega > 0$, $\omega \in (W - \mu + s\omega_0, (s+1)\omega_0)$ with $s \geq 0$, respectively. In these intervals poles in the Green function occur if equation (26) there has a real-valued solution. To be exact, a small width of these peaks can occur due to the third term on the r.h.s. of equation (24) if γ differs appreciable from unity.

2.3. Determination of γ

In order to fix the variational parameter γ self-consistently, we minimise the ground-state expectation value of the Hamiltonian (4)

$$\begin{aligned} \langle \tilde{H} \rangle = & \sum_{k,a} \xi_{ka} \langle c_{ka}^\dagger c_{ka} \rangle - \sum_{ka} \left[\langle C_{ka} \rangle \langle d^\dagger c_{ka} \rangle + \langle C_{ka}^\dagger \rangle \langle c_{ka}^\dagger d \rangle \right] \\ & + \tilde{\eta} \langle d^\dagger d \rangle - \langle C_d \rangle \langle d^\dagger d \rangle + \omega_0 \langle b^\dagger b \rangle \end{aligned} \quad (30)$$

with respect to γ . The first term on the r.h.s. of (30), arising from the leads, is taken to be constant. For the transformed Hamiltonian, $\omega_0 \langle b^\dagger b \rangle$ as well as $\langle C_d \rangle$ is zero for $T \rightarrow 0$ in our second order approach. The remaining expectation values can be expressed as

$$\langle d^\dagger d \rangle = \int_{-\infty}^{\infty} d\omega' A_{dd}(\omega') n_F(\omega'), \quad (31)$$

$$\langle d^\dagger c_{ka} \rangle = G_{cd;ka}(\tau_1, \tau_2) \Big|_{\tau_1 \rightarrow \tau_2^-}, \quad (32)$$

$$\langle c_{ka}^\dagger d \rangle = G_{dc;ka}(\tau_1, \tau_2) \Big|_{\tau_1 \rightarrow \tau_2^-} \quad (33)$$

with G_{cd} resulting from equation (15), where we take the first-order approximation

$$G_{cd;ka}(\tau_1, \tau_2) = -G_{cc;ka}^{(0)}(\tau_1, \tau') \circ \langle C_{ka}^\dagger \rangle G_{dd}(\tau', \tau_2). \quad (34)$$

Again we express the temperature Green functions by a series over Matsubara frequencies and represent the Fourier transforms of G_{dd} , $G_{dd}(i\omega_\nu)$, by the spectral function $A_{dd}(\omega')$. Carrying out the Matsubara summation, we get

$$\langle d^\dagger c_{ka} \rangle = - \langle C_{ka}^\dagger \rangle \int_{-\infty}^{+\infty} d\omega' A_{dd}(\omega') \frac{n_F(\omega') - n_F(\xi_{ka})}{\omega' - \xi_{ka}} \quad (35)$$

and the complex conjugate expression for $\langle c_{ka}^\dagger d \rangle$. Thus, for identical leads and $T \rightarrow 0$, we finally obtain

$$\begin{aligned} \langle \tilde{H} \rangle = & e^{-\tilde{g}^2} \frac{4}{\pi} \left\{ - \int_{-W}^{\mu} d\xi g(\xi) |t(\xi)|^2 \int_0^{+\infty} d\omega' \frac{A_{dd}(\omega')}{\omega' - (\xi - \mu)} \right. \\ & \left. + \int_{\mu}^W d\xi g(\xi) |t(\xi)|^2 \int_{-\infty}^0 d\omega' \frac{A_{dd}(\omega')}{\omega' - (\xi - \mu)} \right\} + \tilde{\eta} \int_{-\infty}^0 A_{dd}(\omega') d\omega', \end{aligned} \quad (36)$$

from which γ is identified by the minimum of $\langle \tilde{H} \rangle(\gamma)$.

2.4. Two-particle properties: kinetic coefficient

In this section we calculate the current of the system (1) caused by a small potential difference between the leads. To this end we deduce the expression for the kinetic coefficient in terms of the quantum-dot spectral function, consistently with the approximations assumed in the derivation of $A_{dd}(\omega)$. In accordance with general linear response theory (Zubarev 1971), the external perturbation $H_t = -\alpha F(t)$ coupled to the system variable α induces the change $\langle \dot{\alpha} \rangle$ of $\langle \alpha \rangle$, whose Fourier transform $\langle \dot{\alpha} \rangle_\omega$ is related to the Fourier component $F(\omega)$ via the kinetic coefficient $L(\omega)$ as

$$\langle \dot{\alpha} \rangle_\omega = L(\omega) F(\omega). \quad (37)$$

In particular, linear response theory gives for $L = L(\omega \rightarrow 0)$ the expression

$$L = \lim_{\omega \rightarrow 0} \left[-\frac{1}{\omega} \text{Im} \langle \langle \dot{\alpha} | \dot{\alpha} \rangle \rangle_\omega \right], \quad (38)$$

where the symbol $\langle \langle \cdot | \cdot \rangle \rangle_\omega$ denotes the retarded (commutator) Green function in frequency representation. In our case, the quantity of interest is the current between the lead a and the dot. By the continuity equation, the operator for this current is

$$J_a = -e \dot{N}_a, \quad (39)$$

where $N_a = \sum_k c_{ka}^\dagger c_{ka}$ and

$$\dot{N}_a = i[H, N_a] = -i \frac{1}{\sqrt{N}} \sum_k \left(t_{ka} \tilde{d}^\dagger c_{ka} - t_{ka}^* c_{ka}^\dagger \tilde{d} \right) \quad (40)$$

with the electron \tilde{d} operators defined in (3). Varying the chemical potential in the second term of the Hamiltonian, presuming $\mu_a = \mu + \Delta\mu_a$, we identify $\alpha = N_a$ and $F = \Delta\mu_a$ in the above general linear response formula.

To obtain the retarded Green function $\langle \langle \dot{N}_a | \dot{N}_a \rangle \rangle$, let us consider the corresponding Matsubara Green function

$$G_J(\tau_1, \tau'_1) = - \left\langle \mathcal{T}_\tau \dot{N}_a(\tau_1) \dot{N}_a(\tau'_1) \right\rangle \quad (41)$$

which is related to the two-particle Green function by

$$G_J(\tau_1, \tau'_1) = \bar{G}(\tau_2, \tau'_2, \tau_1, \tau'_1) \Big|_{\tau_2=\tau_1^-, \tau'_2=\tau'_1}, \quad (42)$$

where

$$\begin{aligned} \bar{G}(\tau_2, \tau'_2; \tau_1, \tau'_1) = \frac{1}{N} \sum_{k, k'} \bigg[& t_{ka} t_{k'a} \left\langle \mathcal{T}_\tau c_{ka}(\tau_2) c_{k'a}(\tau'_2) \tilde{d}^\dagger(\tau'_1) \tilde{d}^\dagger(\tau_1) \right\rangle \\ & - t_{ka} t_{k'a}^* \left\langle \mathcal{T}_\tau c_{ka}(\tau_2) \tilde{d}(\tau'_2) c_{k'a}^\dagger(\tau'_1) \tilde{d}^\dagger(\tau_1) \right\rangle \\ & - t_{ka}^* t_{k'a} \left\langle \mathcal{T}_\tau \tilde{d}(\tau_2) c_{k'a}(\tau'_2) \tilde{d}^\dagger(\tau'_1) c_{ka}^\dagger(\tau_1) \right\rangle \\ & + t_{ka}^* t_{k'a}^* \left\langle \mathcal{T}_\tau \tilde{d}(\tau_2) \tilde{d}(\tau'_2) c_{k'a}^\dagger(\tau'_1) c_{ka}^\dagger(\tau_1) \right\rangle \bigg] \quad (43) \end{aligned}$$

The mean values of all the time-ordered products on the r.h.s. of (43) are basically two-particle Green functions $G(2, 2'; 1, 1')$ (Rickayzen 1981), which may be approximated by one-particle Green functions according to

$$G(2, 2'; 1, 1') \approx G(2, 1)G(2', 1') - G(2, 1')G(2', 1), \quad (44)$$

if vertex corrections due to phonon-mediated electron-electron scattering are neglected. In this way, the terms on the r.h.s. of (43) turn out to be proportional to products of $G_{c\tilde{d}}$, $G_{\tilde{d}c}$, G_{cc} , and $G_{\tilde{d}\tilde{d}}$. Substituting \tilde{d} from (3), averaging over the oscillator variables and inserting the expressions (34) for G_{cd} and $G_{dc} = G_{cd}^*$, it becomes obvious that the terms containing the latter “mixed” Green functions are of higher order in $|\langle C_{ka} \rangle|$. Hence we get as the leading order result

$$\begin{aligned} \bar{G}(\tau_2, \tau'_2, \tau_1, \tau'_1) = \frac{1}{N} \sum_k |t_{ka}|^2 \left[G_{cc; ka}^{(0)}(\tau_2, \tau'_1) \tilde{G}_{dd}(\tau'_2, \tau_1) \right. \\ \left. + \tilde{G}_{dd}(\tau_2, \tau'_1) G_{cc; ka}^{(0)}(\tau'_2, \tau_1) \right]. \end{aligned} \quad (45)$$

Here we have used the unperturbed Green function $G_{cc}^{(0)}$ (see equation (13)) for the electrons in the leads and introduced the notation $\tilde{G}_{dd} = G_{\tilde{d}\tilde{d}}$.

Inserting (45) into (42) and performing a Fourier transformation, the latter equation becomes

$$\begin{aligned} G_J(i\omega_n) = \frac{1}{N} \sum_k |t_{ka}|^2 \frac{1}{\beta} \sum_{\omega_\nu} \left[G_{cc; ka}^{(0)}(i\omega_\nu + i\omega_n) \tilde{G}_{dd}(i\omega_\nu) \right. \\ \left. + G_{cc; ka}^{(0)}(i\omega_\nu) \tilde{G}_{dd}(i\omega_\nu + i\omega_n) \right], \end{aligned} \quad (46)$$

with bosonic Matsubara frequencies $\omega_n = 2n\pi/\beta$. We now express \tilde{G}_{dd} by the electronic spectral function $\tilde{A}_{dd}(\omega)$

$$\tilde{G}_{dd}(i\omega_\nu) = \int_{-\infty}^{\infty} d\omega' \frac{\tilde{A}_{dd}(\omega')}{i\omega_\nu - \omega'}, \quad (47)$$

make use of

$$G_{cc; ka}^{(0)}(i\omega_\nu) = \frac{1}{i\omega_\nu - \xi_{ka}}, \quad (48)$$

perform the Matsubara summation over the fermionic frequencies ω_ν , and obtain

$$\begin{aligned} G_J(i\omega_n) = \frac{1}{N} \sum_k |t_{ka}|^2 \left\{ \int_{-\infty}^{+\infty} d\omega' \tilde{A}_{dd}(\omega') \frac{n_F(\omega') - n_F(\xi_{ka})}{i\omega_n + \omega' - \xi_{ka}} \right. \\ \left. + \int_{-\infty}^{+\infty} d\omega' \tilde{A}_{dd}(\omega') \frac{n_F(\xi_{ka}) - n_F(\omega')}{i\omega_n - \omega' + \xi_{ka}} \right\}. \end{aligned} \quad (49)$$

The analytical continuation of (49), $i\omega_n \rightarrow \bar{\omega} = \omega + i\delta$, gives the retarded Green function

$$\langle\langle \dot{N}_a | \dot{N}_a \rangle\rangle_\omega = G_J(\omega + i0^+), \quad (50)$$

leading to

$$\begin{aligned} \text{Im} \langle\langle \dot{N}_a | \dot{N}_a \rangle\rangle_\omega = -\frac{\pi}{N} \sum_k |t_{ka}|^2 \left\{ \tilde{A}_{dd}(\xi_{ka} - \omega) [n_F(\xi_{ka} - \omega) - n_F(\xi_{ka})] \right. \\ \left. + \tilde{A}_{dd}(\xi_{ka} + \omega) [n_F(\xi_{ka}) - n_F(\xi_{ka} + \omega)] \right\}. \end{aligned} \quad (51)$$

Assuming identical leads $a = l, r$, this result is of course independent of a . Finally, according to the definition (38), we have to perform the limit $\omega \rightarrow 0$:

$$\begin{aligned} L &= \lim_{\omega \rightarrow 0} \left[-\frac{1}{\omega} \text{Im} \langle \langle \dot{N}_a | \dot{N}_a \rangle \rangle_{\omega} \right] = \frac{2\pi}{N} \sum_k |t_{ka}|^2 \tilde{A}_{dd}(\xi_{ka}) (-n'_F(\xi_{ka})) \\ &= 2 \int_{-W}^W d\xi g(\xi) |t(\xi)|^2 \tilde{A}_{dd}(\xi - \mu) (-n'_F(\xi - \mu)) . \end{aligned} \quad (52)$$

Then, for $T \rightarrow 0$, $(-n'_F(\xi - \mu)) = \delta[\xi - \mu]$, so that

$$L = 2g(\mu) |t(\mu)|^2 \tilde{A}_{dd}(0) . \quad (53)$$

The general relation between the electronic spectral function $\tilde{A}_{dd}(\omega)$ and the polaronic spectral function $A_{dd}(\omega)$ determined in the preceding section, was previously derived in Ref. (Loos, Hohenadler & Fehske 2006). Using equation (40) of this work, for $\omega = 0$ and $T \rightarrow 0$, it simply follows that

$$\tilde{A}_{dd}(0) = e^{-\tilde{g}^2} A_{dd}(0) . \quad (54)$$

Consequently, the kinetic coefficient is determined by the value of the polaronic spectral function $A_{dd}(\omega)$ at the lead Fermi level, multiplied with the renormalisation factor $e^{-\tilde{g}^2}$. In particular, changing g , Δ leads to a shift of $A_{dd}(\omega)$ with respect to the lead Fermi level and therefore changes the value of $A_{dd}(0)$, as will be shown by the numerical calculation in the following section.

3. Numerical results

While the derivation of the equations in section 2 is completely general, we consider in the following the case of a single quantum dot between semi-infinite 1D leads, as sketched in figure 1. Accordingly, the density of states of the leads is given by

$$g(\xi) = (2/W) \sqrt{1 - (\xi/W)^2} \Theta(1 - (\xi/W)^2) \quad (55)$$

with the half-bandwidth $W = 2t$. We fix $t = 1$ from here on. The dot-lead transfer $t(\omega)$ (e.g. in equations (24), (25)) is chosen as a constant $t(\omega) = t_d$.

The numerical computation of the Green function $G_{dd}(\bar{\omega})$, equation (22), and the corresponding spectral function $A_{dd}(\omega)$, equations (23), (29), is performed by evaluation of equation (21) for energies $\bar{\omega} = \omega + i\delta$ slightly above the real axis. A small choice of $\delta > 0$ avoids problems arising from the simultaneous treatment of poles and incoherent parts in the Green function. For our computations, we used $\delta \simeq 10^{-3}$. Alternatively, one might directly evaluate equations (24), (25) which are given for real ω , but numerical inaccuracies in the calculation of the principal value integrals tend to degrade the computation. From the spectral function, we obtain the kinetic coefficient L using equations (53), (54).

It is noteworthy that, restricting ourselves to second order perturbation, the approximations to the Green functions preserve important sum-rules for the spectral functions, especially for the integrated weight (Koch 2009). This remains true for finite

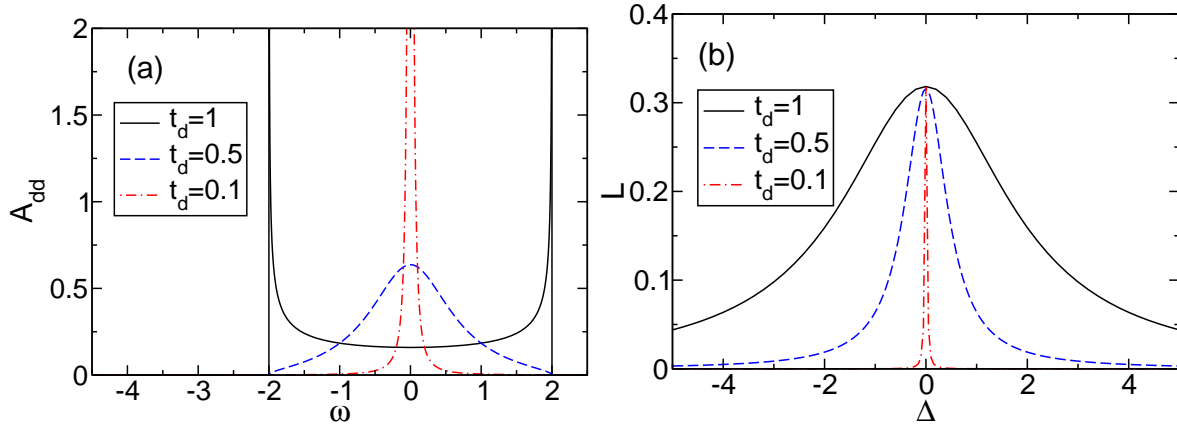


Figure 3. (Colour online) All results for $\varepsilon_p = 0$ and $\mu = 0$. Left panel: Dot spectral function $A_{dd}(\omega)$ for $\Delta = 0$ and several t_d . Right panel: Kinetic coefficient L as a function of Δ for several $t_d = 1$.

$\delta > 0$ in the numerical computation (while the numerically unfavourable evaluation of equations (24), (25) led to the artificial drop of total spectral weight reported in Ref. (Loos, Hohenadler & Fehske 2006)).

In the discussion of the numerical results we start with important limiting cases.

3.1. Non-interacting case

For vanishing EP coupling ($\varepsilon_p = 0$) the problem reduces to that of an impurity in a 1D chain. The spectral function is then obtained exactly by our calculation (left panel in figure 3). For $t_d = 1$, the spectral function of the translationally invariant 1D chain is recovered. For smaller t_d , the spectral function develops a pronounced maximum at $\omega = 0$, which evolves into a δ -peak in the limit $t_d \rightarrow 0$.

For the kinetic coefficient, we observe in figure 3 (right panel) two effects that will be important later in our discussion of the interacting case. First, for dot energy $\Delta \neq 0$ scattering off the dot impurity leads to reduction of L compared to the case $\Delta = 0$ with minimal scattering. Consequently, L is maximal for $\Delta = 0$ and shrinks monotonically with growing $|\Delta|$. Second, a reduction of t_d leads to a reduction of L . Moreover the variation with Δ becomes more pronounced as electrons become more susceptible to scattering off the dot. In equations (24), (25) we see that for smaller hybridisation $t_d^2 g(\xi)$ the broadening of dot levels due to coupling to the continuum of lead states is reduced. In the limit $t_d \rightarrow 0$, the function $L = L(\Delta)$ becomes a δ -function at $\Delta = 0$ with weight $\propto t_d^2$. Note that L is independent of t_d for $\Delta = 0$, which is however a peculiarity of the non-interacting case without damping of states close to the Fermi energy.

3.2. Small phonon frequency

In the following, we first discuss the results of our approach in the limits of small and large (next subsection) phonon frequencies. For the moment, we fix $t_d = t = 1$ and

$\mu = 0$ which corresponds to the half-filled band case for a translational invariant system with $\varepsilon_p = 0$ and $\Delta = 0$.

For small phonon frequency $\omega_0/t = 0.1$ (adiabatic regime), when the phononic timescale is much slower than the electronic timescale, we expect significant deviations from the behaviour described by the standard Lang-Firsov approach consisting of a complete Lang-Firsov transformation and a subsequent average over the transformed phonon vacuum. Our approach is able to account for these deviations by the variational parameter γ . The deviation of γ from unity is some measure of both adiabatic and weak-coupling corrections.

3.2.1. Repulsive dot In figure 4 we show results for the case $\omega_0 = 0.1$, $\mu = 0$, and a repulsive dot $\Delta = 3$. Since the dot is repulsive, the particle density at the dot is small, $n \simeq 0.1$, for small EP coupling ε_p [see panel (b)]. At a critical coupling $\varepsilon_p^c \simeq 3.4$, EP interaction at the dot overcomes the repulsive potential, and a transition takes place to a situation with large n . This transition is accompanied by a jump of the variational parameter γ_{min} from a small value (< 0.02) to 1. This jump can be traced back to the behaviour of the total energy E as a function of γ : If ε_p increases, $E(\gamma)$ develops two local minima [see panel (a)]. At $\varepsilon_p = \varepsilon_p^c$, the minimum at $\gamma = 1$ becomes the new global minimum. Evidently, the sudden change of γ reflects the formation of a strongly localised polaron at the quantum dot. Thereby the lead-dot transfer is almost completely suppressed and, in accordance with this picture, the kinetic coefficient ($\propto \exp\{-g^2\}$) drops to zero at the transition point. This suppression of transport is well described by the complete Lang-Firsov transformation (although this basically is a non-adiabatic approach), mainly because we enter an extreme strong-coupling situation ($g^c = 5.83$). Note that the observation of an extremely sharp polaron transition in the adiabatic regime for repulsive quantum dots is in accordance with recent exact diagonalisation results (Fehske et al. 2008, Alvermann & Fehske 2008).

We next analyse the dot spectral function A_{dd} [see figure 4 (c)-(d)]. For $\varepsilon_p < \varepsilon_p^c$, we have $\tilde{g} \leq \gamma_{min}g^c < 0.1166$ and, calculating $\Sigma_{dd}^{(1)}$ within our second order scheme, the first term in equation (21) is basically proportional to the semi-elliptical density of states of the leads, while the second term (“phononic contribution”) is insignificant. Then the resulting spectral function $A_{dd}^{(1)}$, which has to be put into the third term of (21), describes a continuum of states, roughly inbetween -2 and 2, and a localised dot state at $\omega \simeq 3.5$ (in accordance with the result obtained for the Fano-Anderson model). Since the prefactor of the third term, $(1 - \gamma_{min})g\omega_0 \lesssim 0.57$ for $g \leq g^c$, is rather large this term gives a significant contribution to the second order self-energy Σ_{dd} . Thereby the localised peak in $A_{dd}^{(1)}$ becomes evident in Σ_{dd} [see inset of figure 4 (c)]. As a result the second order spectral function, A_{dd} , exhibits two sharp peak structures (localised states) above the continuum of states around $\omega = 0$. If the EP coupling increases these peaks become more and more separated. In order to analyse the spectral weight of the

different signatures in A_{dd} , we have calculated the integrated spectral function

$$S(\omega) = \int_{-\infty}^{\omega} d\omega' A_{dd}(\omega'). \quad (56)$$

Figures 4 (c) and (d) show that for $\varepsilon_p < \varepsilon_p^c$ the spectral weight mainly rests in the localised peak structures above the wide band. Hence the spectral weight of the current-carrying states at the Fermi energy $\mu = 0$ is reduced, and the kinetic coefficient $L \propto A_{dd}(0)$ is substantially lowered compared to the case $\Delta = 0$. At $\varepsilon_p = \varepsilon_p^c$, γ_{min}

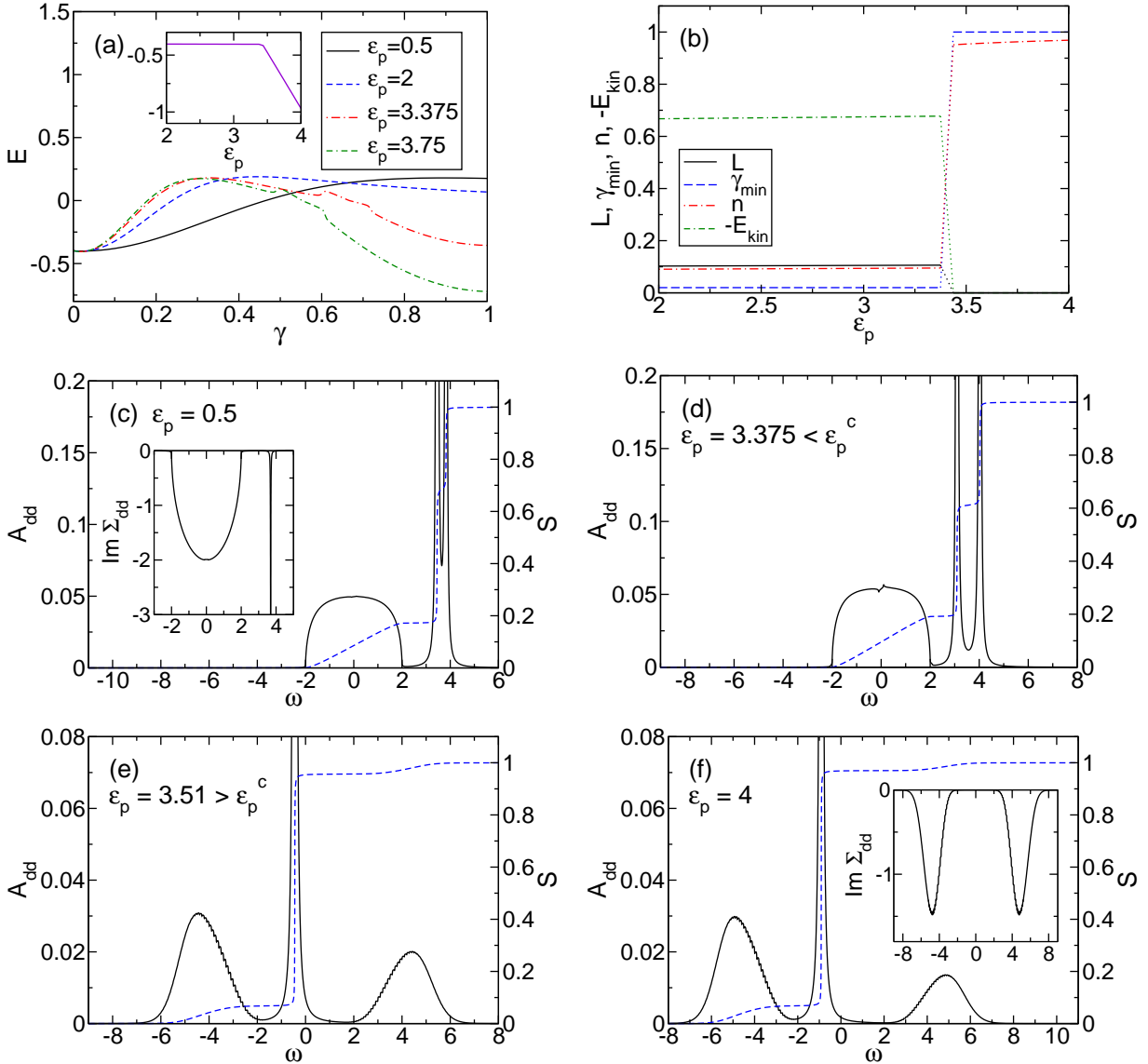


Figure 4. (Colour online) All results for $\Delta = 3$, $t = t_d = 1$, $\mu = 0$, and $\omega_0 = 0.1$. Upper panels: Total energy E (a) as a function of γ , for different ε_p (inset: Minimum of E as a function of ε_p) and optimal parameter γ_{min} , kinetic coefficient L , particle density n at the dot, and kinetic energy E_{kin} (b) as a function of ε_p . Lower panels: Dot spectral function $A_{dd}(\omega)$ and integrated spectral weight $S(\omega)$ for different ε_p (c)-(f). The insets in panels (c) and (f) show the imaginary part of the second-order self-energy $\Sigma_{dd}(\omega)$.

jumps to 1, and the strong renormalisation arising from the complete Lang-Firsov-transformation results in a pronounced peak at negative energy at about $\Delta - \varepsilon_p$, which now, however, is the signature of a quasi-localised polaronic dot state. The polaronic quasiparticle peak is accompanied by two side-bands, roughly of width $2W$ and shifted by $\pm\varepsilon_p$, which arise from the Poissonian distribution of phonons at the dot, with maximum at $g^2 = \varepsilon_p/\omega_0$ phonons corresponding to energy $\omega_0 g^2 = \varepsilon_p$. States in these band are strongly damped due to the significant phononic admixture, as is evident in the imaginary part of the self-energy [see inset figure 4 (f)].

3.2.2. The case $\Delta = 0$ For $\Delta < 0$ the quantum dot is attractive. For $\Delta = 0$ and $\varepsilon_p = 0$ we have of course a translational invariant 1D system, where $\mu = 0$ corresponds to the half-filled band case, i.e., $n = 0.5$. Such a “neutral” quantum dot becomes attractive for arbitrarily weak EP interaction. This is because the “effective” dot level is given by $\tilde{\eta} = \Delta - \varepsilon_p \gamma_{min}(2 - \gamma_{min})$.

Consequently, in figure 5 (b) the particle density at the dot is larger than 0.5 for all ε_p , and the dot spectral function has no pole at positive energies. At small EP coupling the spectral function is similar to that of a 1D tight-binding model. The weak EP interaction causes the spiky signatures separated by ω_0 from the upper and lower band edges [see figure 5 (c)]. In contrast to a repulsive dot, for which our methods correctly describes the transition from unbound to localised polaronic dot states, a sharp polaron transition cannot occur for a dot level $\Delta \leq 0$. Nevertheless, we observe in figure 5 a transition signalled by the jump of γ_{min} to 1 with corresponding increase of n , decrease of L , and formation of a pronounced peak in $A_{dd}(\omega)$ at negative energies. The reason is again the change of the global minimum of $E(\gamma)$, which has two local minima for larger ε_p . Since for $\Delta = 0$ the interaction need not overcome a repulsive dot potential, the transition takes places at smaller $\varepsilon_p^c \approx 1.4$. Therefore, and in contrast to the previous case, no isolated quasiparticle peak in $A_{dd}(\omega)$ emerges at the transition, and the change of the spectral function is less dramatic. Above the transition the qualitative behaviour of the imaginary part of the self-energy [see inset of 5 (f)] is the same as for the repulsive quantum dot [cf. inset of 4 (f)]. Since the mean phonon number $g^2 \simeq 15$ involved is smaller now, however, the maxima of the phonon contributions to Σ_{dd} are less separated.

In our approach the transition results from a jump in γ_{min} . As before, this might indicate the formation of a localised polaronic dot state. But we know from the various variational approaches to the polaron problem that such jumps often arise as artefacts of the variational ansatz (Fehske et al. 1994). For the Holstein polaron with EP interaction at each lattice site, no phase transition exists (Gerlach & Löwen 1991). Instead, a crossover between an almost free electron and a heavy polaron takes place. The crossover can however be very rapid for small phonon frequency (Alvermann et al. 2008). But we also know that, in contrast to the Holstein polaron problem, for a single electron at a vibrating quantum dot a true phase transition, from $n = 0$ to finite $n > 0$, takes place (Mishchenko et al. 2009, Alvermann & Fehske 2008, Fehske et al. 2008). This phase transition becomes more pronounced for small ω_0 . The behaviour found here

therefore does not contradict the essential physical mechanism in our situation. In principle, our approach mimics the sharp adiabatic polaron transition by the change of the parameter γ of the (non-adiabatic) Lang-Firsov transformation. While the precise nature of the transition is only poorly described by this approximation, we still believe that the transition – or rapid crossover – itself is characteristic for the quantum dot at small ω_0 .

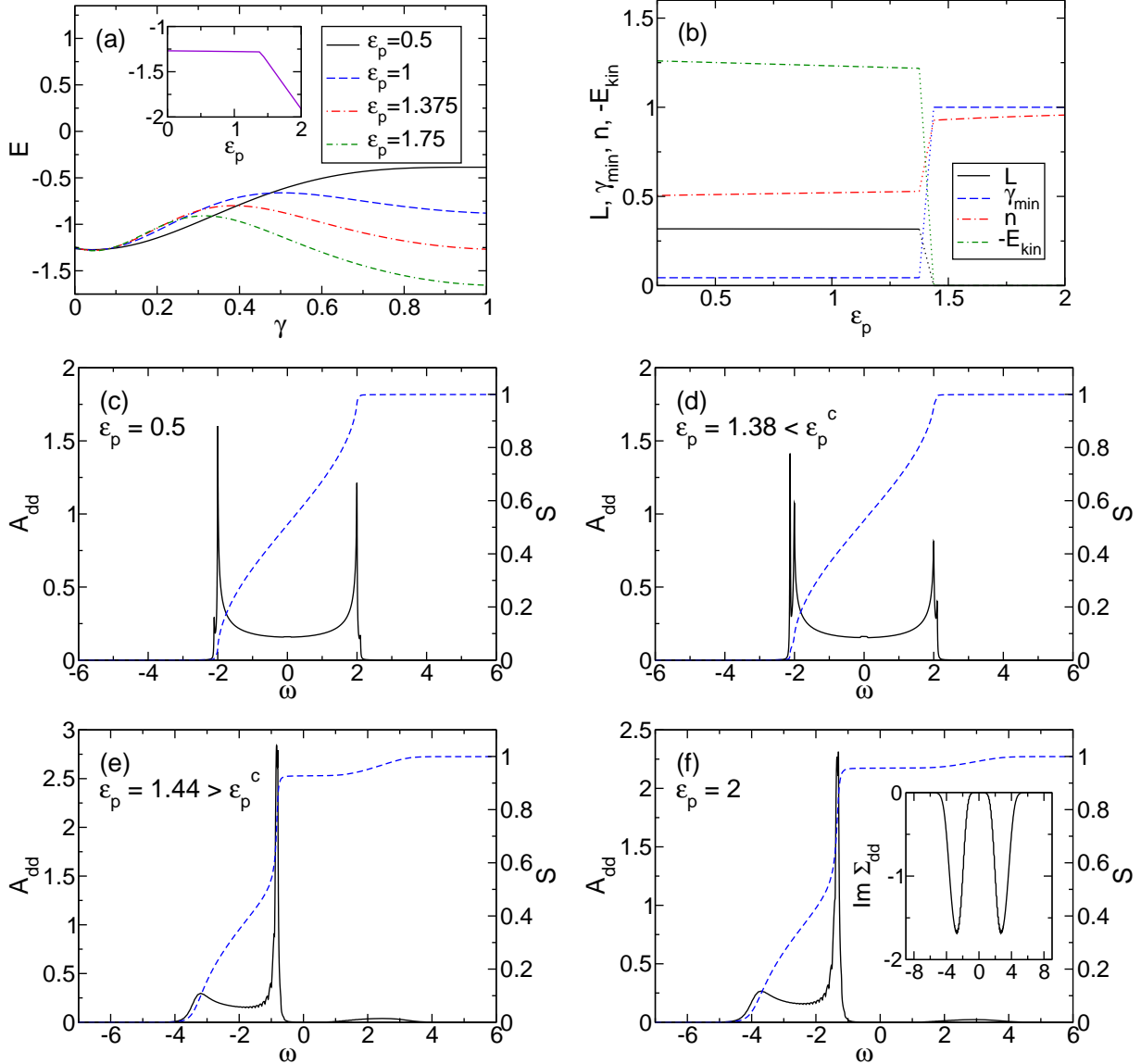


Figure 5. (Colour online) All results for $\Delta = 0$, $t = t_d = 1$, $\mu = 0$, and $\omega_0 = 0.1$. Upper panels: Total energy E (a) as a function of γ , for different ϵ_p (inset: Minimum of E as a function of ϵ_p) and optimal parameter γ_{\min} , kinetic coefficient L , particle density n at the dot, and kinetic energy E_{kin} (b) as a function of ϵ_p . Lower panels: Dot spectral function $A_{\text{dd}}(\omega)$ and integrated spectral weight $S(\omega)$ for different ϵ_p (c)-(f). The inset in panel (f) gives the imaginary part of the dot self-energy $\Sigma_{\text{dd}}(\omega)$.

3.3. Large phonon frequency

For large phonon frequency $\omega_0 = 10$, in the antiadiabatic regime, phonons adjust instantaneously to the electrons. Now our non-adiabatic variational Lang-Firsov approach perfectly matches the situation. We will see that the transitions found in the previous (adiabatic) cases will be replaced by smooth changes of the physical observables. We then note that the results obtained can be understood easily starting from the case without EP interaction.

3.3.1. Repulsive dot The fact that for large phonon frequency no transitions occur is most clearly seen for a repulsive barrier in figure 6: All quantities depend smoothly on ε_p . The total energy $E(\gamma)$ has a unique minimum for all ε_p , which is the reason why no transition occurs. Note that γ grows from ≈ 0.75 to 1, as ε_p is increased. For large ω_0 and ε_p , the Lang-Firsov transformation implements the correct physical mechanisms. Nevertheless, at weak EP coupling, the deviation $\gamma < 1$ indicates the importance of corrections to the complete Lang-Firsov transformation.

The spectral functions in figure 6 show that, although no transition occurs, we start with a peak in $A_{dd}(\omega)$ at positive energies for small ε_p ($< \Delta$), to end up with a polaronic quasiparticle signature at very strong EP coupling. At $\varepsilon_p = 2$, the peak enters the band of lead states from above, leading to an asymmetric deformation of the semi-elliptic band [see panel (c)]. A second absorption feature is separated by the phonon frequency, but carries almost no spectral weight. With, increasing EP interaction, the effective dot level is lowered until a “neutral” dot evolves at about $\tilde{\eta} = \Delta - \varepsilon_p = 0$, as can be seen from the 1D tight-binding-model-like absorption in panel (d) (note that we here are in the weak EP interaction regime since $g^2 = 0.3$, which is the relevant coupling parameter in the anti-adiabatic region, is small). At large EP coupling, the polaronic peak appears at $\tilde{\eta} < 0$ and acquires a spectral weight of nearly unity (see panel (f) for $\varepsilon_p = 8$). Due to the large phonon frequency $\omega_0 > W$, the phononic sidebands do not overlap in this case (in contrast to figure 4), and the spectral function and self-energy show the typical multi-band structure known from the antiadiabatic Holstein polaron. Most importantly, inbetween the non-overlapping phonon (side) bands, we now have intervals where $\text{Im}\Sigma_{dd} = 0$. If the polaronic peak is located within such an intermediate range the quasiparticle cannot decay by (multi-) phonon absorption or emission processes [see panel (f)]. This means the polaronic dot state acquires in principle an infinite lifetime (in the limit of very large couplings and phonon frequency). Naturally, as $\omega_0 \rightarrow \infty$, we recover the behaviour of the impurity model, where a true bound state occurs (Alvermann & Fehske 2008, Mishchenko et al. 2009).

Thus, for large phonon frequency, or whenever γ is close to unity, we can understand most properties starting from the non-interacting case, if we take the interaction into account by renormalisation of the appropriate physical parameters. Inspection of equations (53), (54) shows that one central effect of interaction on the kinetic coefficient is the renormalisation of t_d to an effective dot-lead hopping $t_d e^{-\tilde{g}^2/2}$. The second central

effect is the change in the dot density of states, which is to a large extent caused by lowering of the effective dot energy (below the value Δ without interaction) due to deformation of the quantum dot in the presence of electrons.

The simplest picture is valid only in the limit $\gamma = 1$, when the dot energy is effectively lowered by $-\varepsilon_p$, such that $\tilde{\eta} = \Delta - \mu - \varepsilon_p$ in equation (6), and the dot-lead hopping is effectively reduced by $e^{-g^2/2}$, such that $\tilde{A}_{dd}(0) = e^{-g^2} A_{dd}(0)$ in equation (54). The kinetic coefficient L then has properties analogous to the non-interacting case, with the appropriately renormalised parameters. We discussed above (section 3.1) the

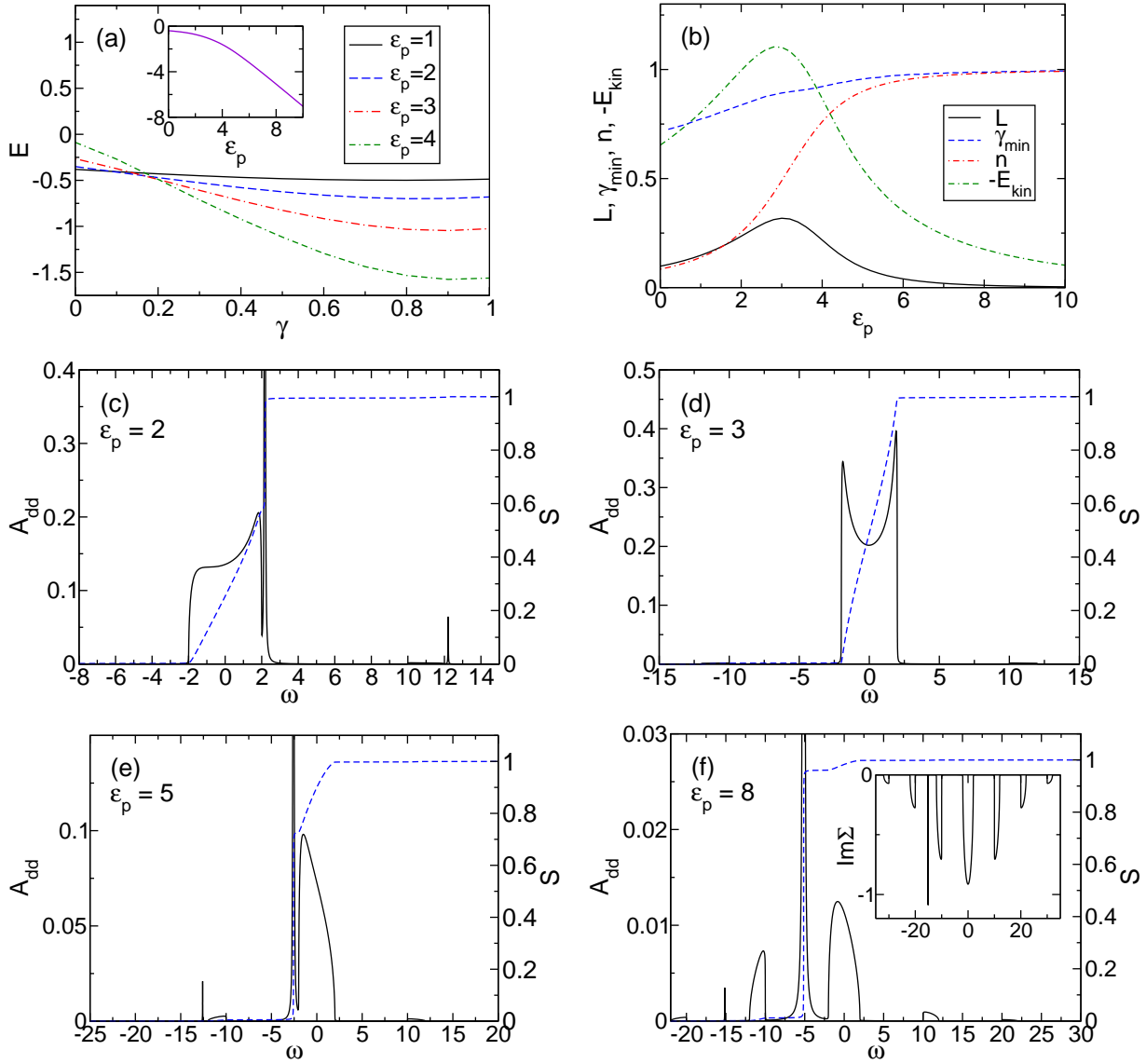


Figure 6. (Colour online) All results for $\Delta = 3$, $t = t_d = 1$, $\mu = 0$ and $\omega_0 = 10$. Upper panels: Total energy E (a) as a function of γ , for different ε_p (inset: Minimum of E as a function of ε_p) and optimal parameter γ_{\min} , kinetic coefficient L , particle density n at the dot, and kinetic energy E_{kin} (b) as a function of ε_p . Lower panels: Dot spectral function $A_{dd}(\omega)$ and integrated spectral weight $S(\omega)$ for different ε_p (c)-(f). The inset in panel (f) gives the imaginary part of the dot self-energy $\Sigma_{dd}(\omega)$.

consequences for L resulting from a change of t_d or Δ . For the curve shown in figure 6, it turns out that it can be indeed reproduced from the expression for L in the non-interacting case, evaluated with an effective dot energy $\Delta - \varepsilon_p$ and effective dot lead hopping $\tilde{t}_d = t_d e^{-g^2/2}$ replacing Δ , t_d . In particular, L is maximal for $\varepsilon_p = \Delta$ (cf. figure 3). Note that away from the limit of large phonon frequency, whenever $\gamma \ll 1$, different behaviour is found. Also the shape of the dot spectral function, and especially the value of $A_{dd}(0)$, is modified in addition to simple renormalisation. Of course, and similar as for the polaron problem, the retardation of the EP interaction manifests itself most prominently at small to intermediate phonon frequency.

3.3.2. The case $\Delta = 0$ The behaviour for the attractive dot is similar to the previous case (see figure 7). Here, of course, a pronounced peak in $A_{dd}(\omega)$ occurs at negative energies for all ε_p . Once again, all features can be understood starting from the non-interacting case with appropriate renormalisation, as explained above. Since $\tilde{\eta} \leq 0$ for all $\varepsilon_p \geq 0$, the kinetic coefficient has no maximum as a function of ε_p .

The simple picture given above consists of both the renormalisation of t_d and Δ . It is important to keep in mind that both effects lead to a reduction of L . As a consequence, the change of the kinetic coefficient is not simply given by an exponential behaviour $\propto e^{-g^2}$ (compare L to the dashed curve in figure 7). In the present case, the coupling strength is small in terms of the average number of phonons $g^2 = \varepsilon_p/\omega_0$, for which $g^2 < 1$, but large in terms of the shift of the dot energy ε_p , which is of the order of the bandwidth W . Here, the reduction of L is mainly caused by this large shift.

The opposite situation can occur for small phonon frequency, when g^2 is large already for small ε_p . Then, however, the renormalisation of t_d is not adequately described by an exponential factor $e^{-g^2/2}$. In the limit $\omega_0 \rightarrow 0$ of small phonon frequency, $g^2 = \varepsilon_p/\omega_0 \rightarrow \infty$ for any $\varepsilon_p > 0$. If the exponential dependence $\propto e^{-g^2}$ persisted, that would imply zero current even for tiny ε_p , which is unphysical. A calculation with fixed $\gamma = 1$ therefore overestimates the reduction of L for intermediate-to-small phonon frequencies. We discussed in the previous subsection how, in our treatment, variation of the parameter γ accounts partially for this deviation, leading to $\gamma \ll 1$ away from the antiadiabatic strong-coupling limit.

3.4. Intermediate phonon frequency

For intermediate phonon frequencies the qualitative behaviour depends crucially on the value of γ , even if no transition occurs. From our previous discussion we know that both a positive Δ or a small ω_0 favour a rapid, or even discontinuous, transition. For $\omega_0 = 1$, we show in figure 8 (upper row) how a smooth crossover evolves into a sudden transition with increasing Δ . In contrast to the case of small phonon frequency $\omega_0 = 0.1$, the kinetic coefficient L is a smooth function of ε_p for $\Delta = 0$. A transition in L occurs only for larger Δ . Increasing the phonon frequency to $\omega_0 = 3$ [lower row, panel (c)] then leads again to a smooth crossover even at $\Delta = 3$.

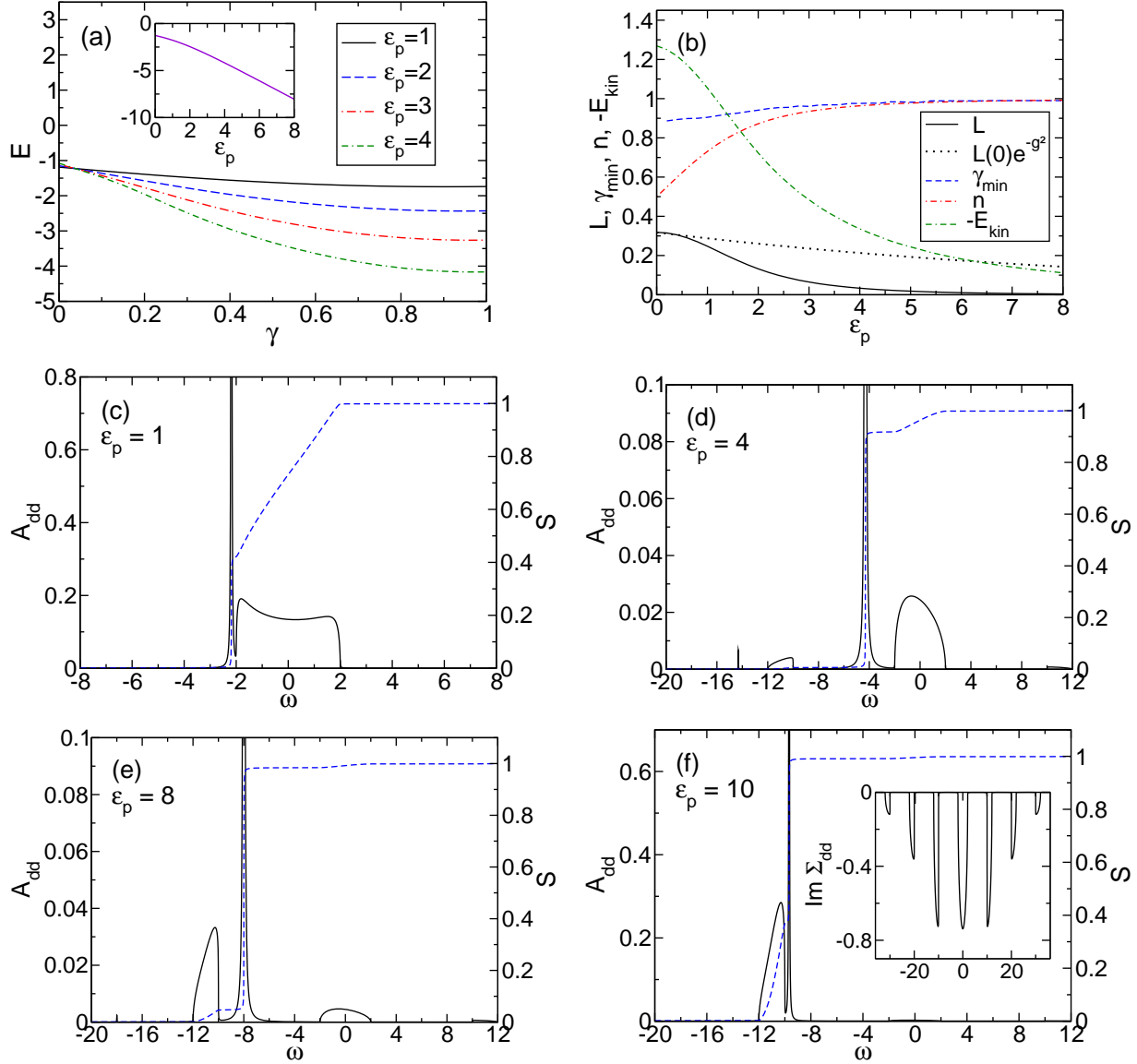


Figure 7. (Colour online) All results for $\Delta = 0$, $t = t_d = 1$, $\mu = 0$ and $\omega_0 = 10$. Upper panels: Total energy E (a) as a function of γ , for different ϵ_p (inset: Minimum of E as a function of ϵ_p) and optimal parameter γ_{\min} , kinetic coefficient L , particle density n at the dot, and kinetic energy E_{kin} (b) as a function of ϵ_p . Lower panels: Dot spectral function $A_{\text{dd}}(\omega)$ and integrated spectral weight $S(\omega)$ for different ϵ_p (c)-(f). The inset in panel (f) gives the imaginary part of the dot self-energy $\Sigma_{\text{dd}}(\omega)$.

With respect to the change of behaviour with phonon frequency, we should ask to which extent the renormalisation scenario given for the antiadiabatic case remains applicable. For $\omega_0 = 3$ [panel (c)] we observe that L differs from the value obtained, as in the previous subsection, from the non-interacting case for renormalised Δ , t_d (in particular the maximum of L occurs for $\epsilon_p > \Delta$), but although $\Delta = 3$, the two curves match rather well. The situation changes for $\omega_0 = 1$ [panel (d)], where strong deviations occur already for $\Delta = 0$ (note that the dashed curve for $\Delta = 2$ even misses the increase of L at smaller ϵ_p). Evidently, the simple renormalisation scenario fails, as

we expected. We can achieve much better agreement if we perform the same calculation but incorporate the parameter γ taken from the upper left panel in figure 8 (the dashed curves would correspond to fixed $\gamma = 1$). Small deviations remain for $\Delta = 2$, since the full calculation includes damping of states, indicated by a finite imaginary part of the self-energy, which is not captured by the change of γ .

It is now evident that the essential feature of our calculation is the self-consistent determination of the parameter γ . Once we know its value, we may get a good approximation already with a modified renormalisation argument which was originally constructed for the antiadiabatic limit. If, in contrast, we fix $\gamma = 1$ we will miss the physics away from the limit of large phonon frequencies. The restricted use of the Lang-Firsov transformation for intermediate-to-small phonon frequencies is well known in the Holstein polaron literature. It is important to realize that this restriction applies also to the situation of a vibrating quantum dot.

3.5. Variation of the chemical potential

So far all results were given for chemical potential $\mu = 0$. A change of the chemical potential affects the kinetic coefficient in two ways. First, since in equation (53) the lead density of states $g(\xi)$ and the dot spectral function $A_{dd}(\omega)$ are evaluated at the chemical potential, a change of μ results in a change of L . Second, phonon emission/absorption is possible only if free states are accessible after an electron changed its energy by $\pm s\omega_0$. Otherwise, EP interaction is suppressed by Pauli blocking. Therefore, the shape of $A_{dd}(\omega)$ itself does depend on μ in a true many-particle calculation as performed here. Significant changes occur whenever $\pm\omega$ crosses the band edges (at about $\pm W - \mu$ at weak coupling).

This effect is evident in the spectral function $A_{dd}(\omega)$ in figure 9. At weak coupling ($\varepsilon_p = 0.5$) the shape of $A_{dd}(\omega)$ is similar for half-filling ($\mu = 0$) and small particle density ($\mu = -1.9$), but small differences at the lower band edge are a first indication of the different behaviour at stronger coupling. There, for $\varepsilon_p = 3.1$, the spectrum for $\mu = 0$ is completely incoherent, with finite $\text{Im } \Sigma_{dd}(\omega)$. Around $\omega = 0$ we observe a valley in $\text{Im } \Sigma_{dd}(\omega)$ of width $2\omega_0$, which results from Pauli blocking of states in the vicinity of the Fermi energy (cf. the discussion in Ref. (Loos, Hohenadler & Fehske 2006)). Note that $\text{Im } \Sigma_{dd}(\omega) \neq 0$ here even at the Fermi energy, since the self-energy contains the contribution from dot-lead transfer. For $\mu = -1.9$, states below the phonon emission threshold, located ω_0 above the lower band edge, cannot emit a phonon (phonon absorption is suppressed at zero temperature). Electrons in these states are undamped, with infinite lifetime corresponding to $\text{Im } \Sigma_{dd}(\omega) = 0$.

The interpretation of the behaviour of the kinetic coefficient L (see figure 10) relies on these two mechanism. First, if μ decreases, the change in the density of states should reduce the value of L [compare the curves for $\mu = 0$ (solid line) and $\mu = -1.9$ (dot-dashed line)]. Also, the dot density of states n decreases. We note that for the non-interacting ($\varepsilon_p = 0$) 1D case the changes in $g(\xi)$ and $A_{dd}(\omega)$ cancel by chance, and

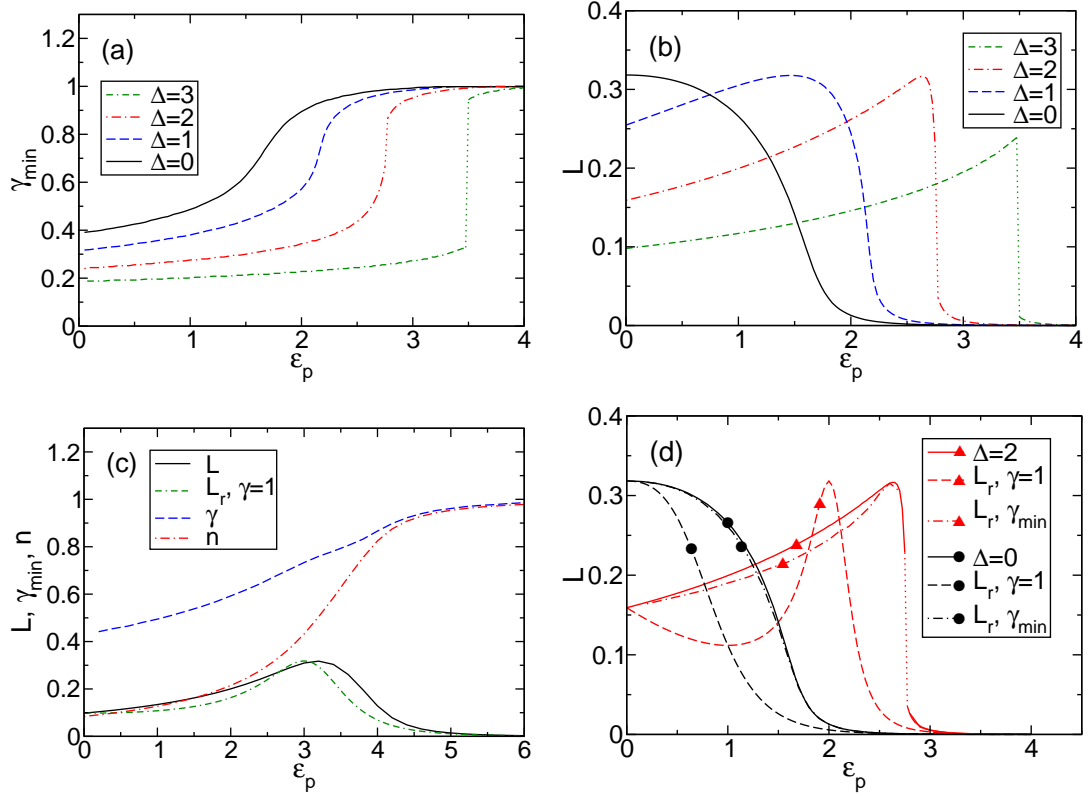


Figure 8. (Colour online) All results for $t = t_d = 1$, $\mu = 0$. Upper row: For $\omega_0 = 1$, optimal γ_{min} (a) and kinetic coefficient L (b) for various Δ as indicated. Lower row, panel (c): For $\Delta = 3$ and $\omega_0 = 3$, optimal parameter γ_{min} , kinetic coefficient L , and particle density n at the dot, as a function of ε_p . The dashed green curve shows L calculated for the non-interacting case with renormalised parameters (see text). Lower row, panel (d): For $\omega_0 = 1$ and two different Δ , kinetic coefficient L as a function of Δ . The dashed curves show L calculated for the non-interacting case with renormalised parameters, but fixed $\gamma = 1$. The dot-dashed curves have been obtained taking the parameter γ from the upper left panel (see text).

L is independent of μ . However, at stronger coupling, the different influence of Pauli blocking reverses this behaviour, and L is larger for smaller μ . This explains why the curve for $\mu = -1.9$ crosses the other two curves in figure 10.

3.6. Small dot-lead hopping (tunnel contacts)

We have so far discussed the importance of the phonon frequency only in the situation $t = t_d$. On physical grounds it is the ratio ω_0/t_d , instead of ω_0/t , which should distinguish the adiabatic from the antiadiabatic regime.

In figure 11 we show, for intermediate phonon frequency $\omega_0 = 1$ and $\Delta = 0$, the change of behaviour as t_d is reduced by one order of magnitude. Reduction of t_d also reduces the conductivity, and the kinetic coefficient L decreases with t_d (see upper panels). Note that if we reduce t_d at fixed $\lambda = \varepsilon_p/(2t_d)$ in figure 11 (a), we

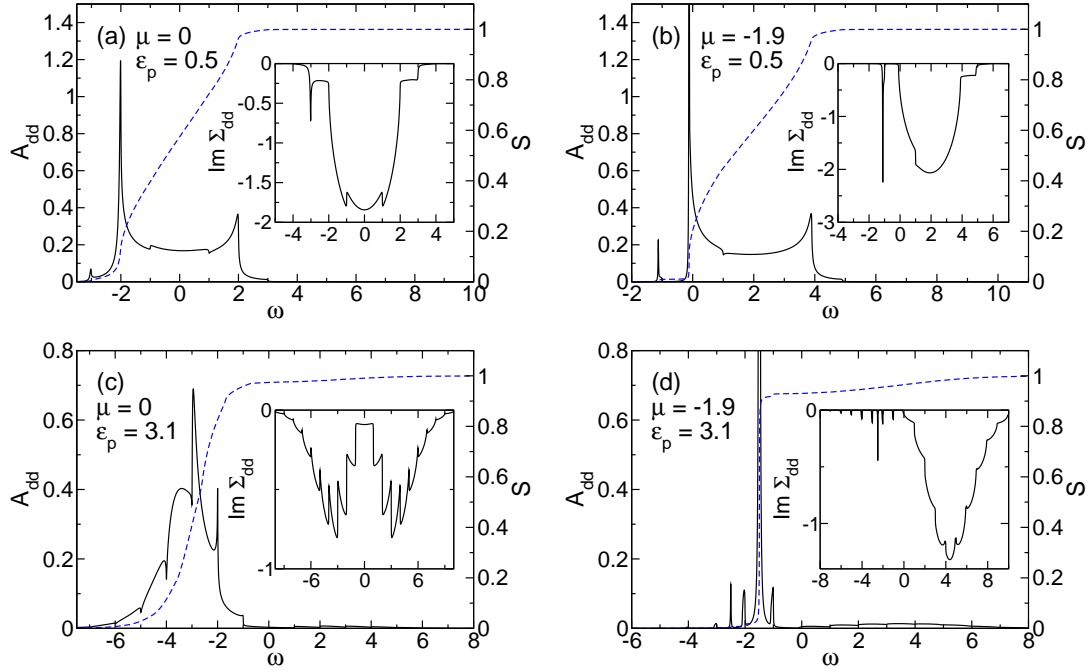


Figure 9. (Colour online) All results for $\Delta = 0$, $t = t_d = 1$ and $\omega_0 = 1$. Comparison of $A_{dd}(\omega)$, $S(\omega)$, and the self-energy $\Sigma_{dd}(\omega)$ (insets) for $\mu = 0$ [left column, panels (a) and (c)] and $\mu = -1.9$ [right column, panels (b) and (d)], for weak coupling $\varepsilon_p = 0.5$ [upper row, panels (a) and (b)] and strong coupling $\varepsilon_p = 3.1$ [lower row, panels (c) and (d)].

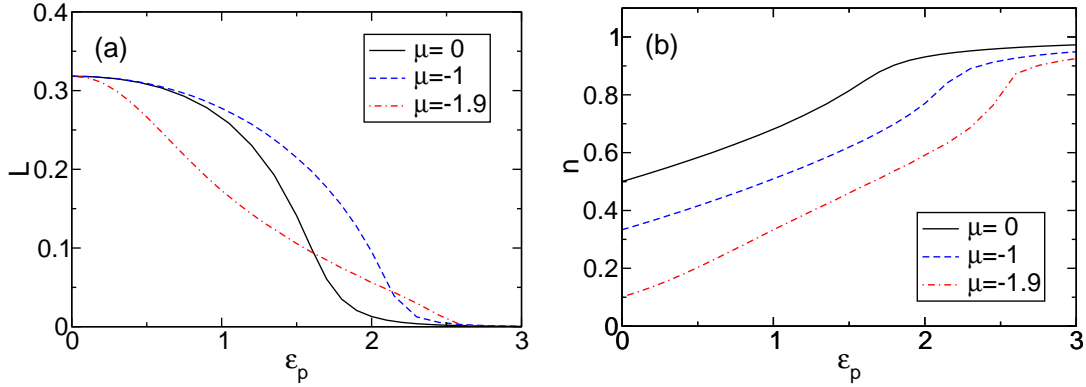


Figure 10. (Colour online) All results for $\Delta = 0$, $t = t_d = 1$ and $\omega_0 = 1$. Kinetic coefficient L [panel (a)] and dot density of states n [panel (b)] as a function of ε_p , for varying chemical potential μ .

de facto reduce the coupling ε_p , but nevertheless L decreases. This implies that the effect of smaller t_d on L dominates over the possible increase of L for smaller coupling. We compare L again with the value obtained in the renormalisation scenario, with a calculation as in the non-interacting case but with renormalised parameters Δ , t_d (see dashed lines). For $t_d = t = 1$, and $\omega_0/t_d = 1$, both curves disagree. We already discussed above that this is a consequence of adiabatic corrections, which become important at intermediate-to-small phonon frequency. However, if we reduce t_d to 0.1 while keeping

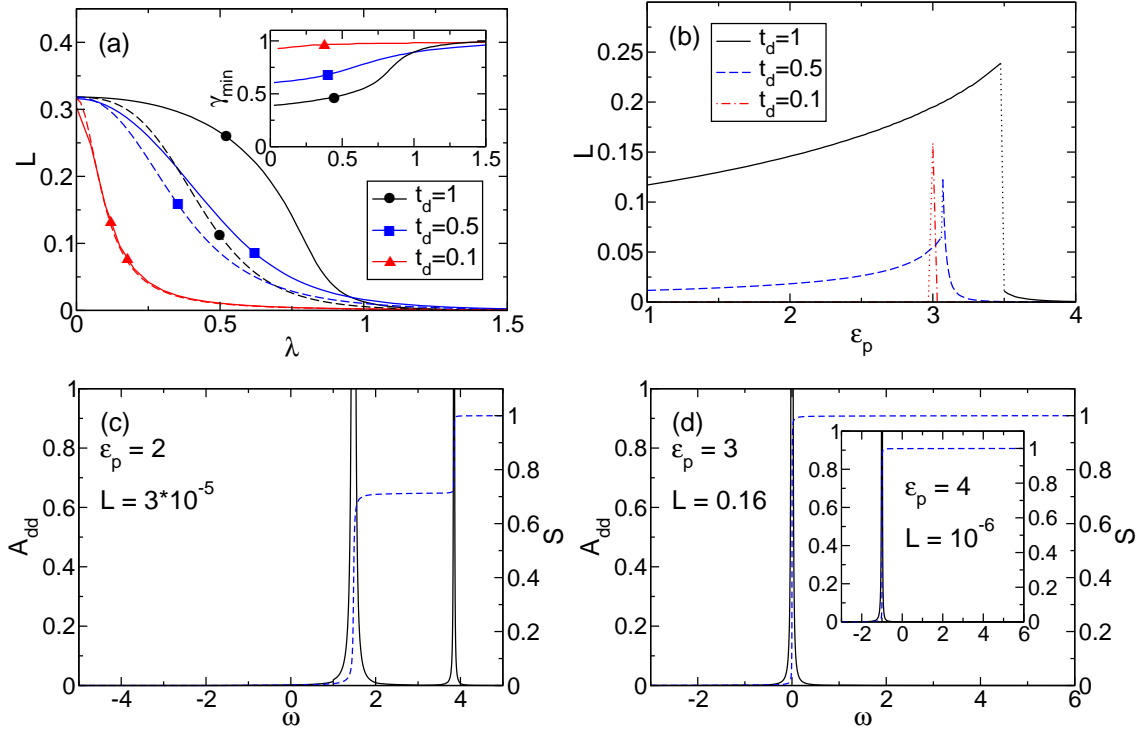


Figure 11. (Colour online) All results for $t = 1$, $\mu = 0$ and $\omega_0 = 1$. Upper row: Kinetic coefficient L as a function of $\lambda = \varepsilon_p/2t_d$ at $\Delta = 0$ [panel (a)] and as a function of ε_p at $\Delta = 3$ [panel (b)] for different t_d . In panel (a) L is compared to the renormalised non-interacting case (dashed lines, see text). The inset in panel (a) gives the corresponding optimal parameter γ_{min} . Lower row: Dot spectral function $A_{dd}(\omega)$ and integrated spectral weight $S(\omega)$ at $\Delta = 3$, $t_d = 0.1$ for $\varepsilon_p = 2$ (c), $\varepsilon_p = 3$ (d), and $\varepsilon_p = 4$ [inset, panel (d)].

$\omega_0 = 1$ fixed, and thereby increase ω_0/t_d to 10, both curves match. Apparently, we enter the antiadiabatic regime by sufficient reduction of t_d . This indicates that indeed ω_0/t_d is the relevant ratio to distinguish the adiabatic from the antiadiabatic regime. For $\omega_0/t_d \gg 1$, and independent of ω_0/t , the system has physical properties that can be described within the simple renormalisation scenario associated with the complete Lang-Firsov transformation.

In figure 11 (b) we make the same observation for $\Delta = 3$, still with $\omega_0 = 1$. For $t_d \gtrsim 0.5$ the kinetic coefficient L shows the transition familiar to us from the previous discussions of intermediate or small phonon frequencies, which is in contrast to the physics in the antiadiabatic regime. For $t_d \ll 1$ a sharp peak occurs in L for $\varepsilon_p = \Delta$. This is of course the behaviour expected for the antiadiabatic regime, which is reminiscent of the non-interacting case for small t_d with a peak of L at $\Delta = 0$ (cf. figure 3).

The lower panels of figure 11 show the spectral function of the repulsive quantum dot at small dot-lead hopping $t_d = 0.1$ for $\tilde{\eta} > 0$ [panel (c)], $\tilde{\eta} \simeq 0$ [panel (d)], and $\tilde{\eta} < 0$ [inset panel (d)]. Below the “critical” EP coupling we have $\gamma_{min} \simeq 0.2$ and obtain a double-peak structure of A_{dd} because both the first and the third term in

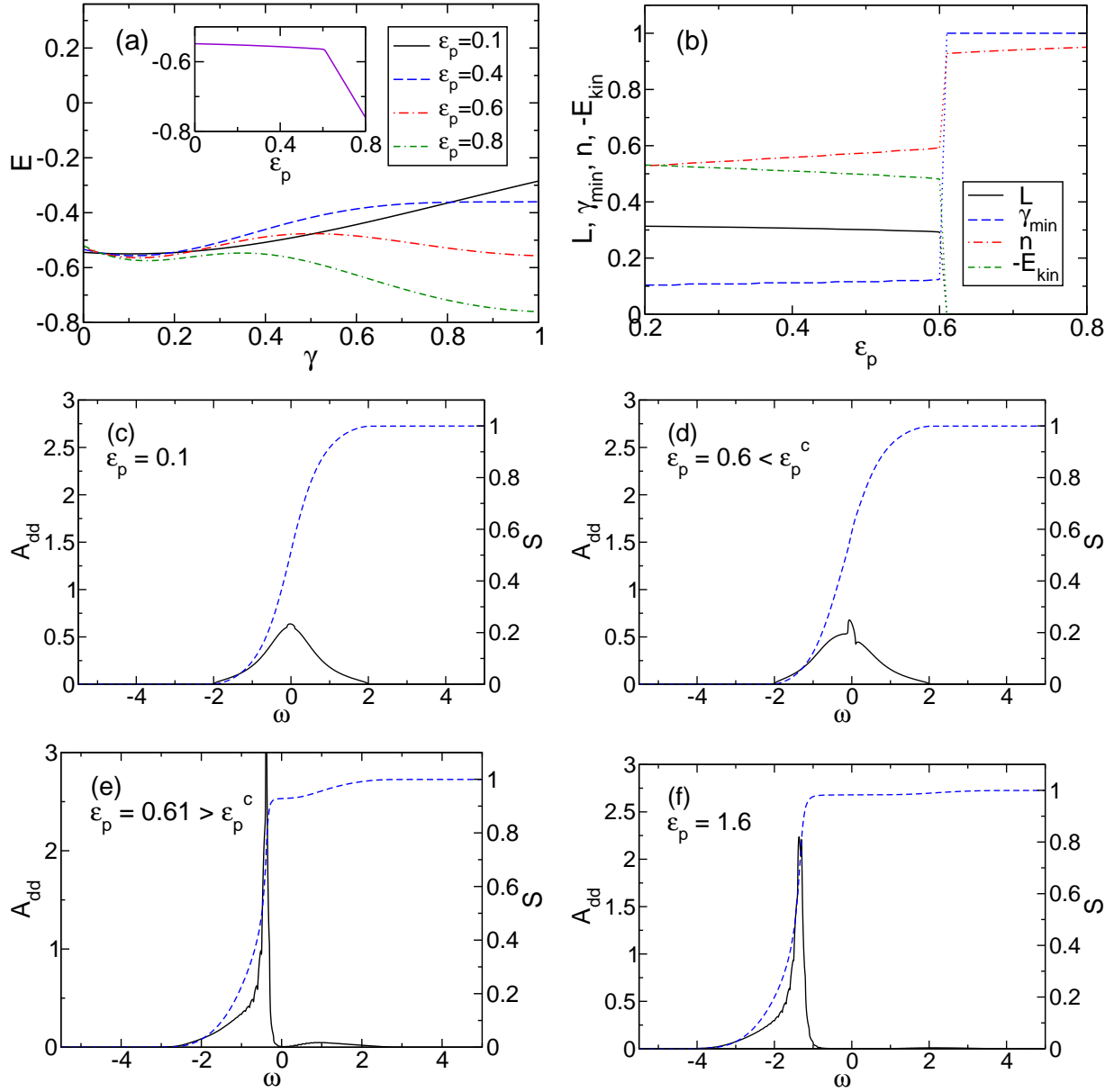


Figure 12. (Colour online) All results for $t = 1$, $\Delta = 0$, $t_d = 0.5$, $\mu = 0$, and $\omega_0 = 0.1$. Panel (a): E as a function of γ for different ϵ_p (inset: minimum of E as a function of ϵ_p). Panel (b): L , γ_{\min} , n and E_{kin} as functions of ϵ_p . For $\epsilon_p^c \approx 0.605$ a crossover takes place. (c)-(f) Spectral functions $A_{\text{dd}}(\omega)$ and integrated spectral weight $S(\omega)$ for coupling strengths below and above ϵ_p^c .

equation (21) give significant contributions. At $\epsilon_p = 3$, the prefactor of the third term vanishes ($\gamma_{\min} = 1$), and a single-peak structure develops. This polaronic peak is located at the Fermi energy and contains all the spectral weight. Therefore L is enlarged more than three orders of magnitude. Increasing ϵ_p further the polaronic signal is narrowed and shifted away from the Fermi level. As a result L decreases off by five orders of magnitude.

Figure 12 gives more results for the experimentally relevant wide-band case, $t > t_d$,

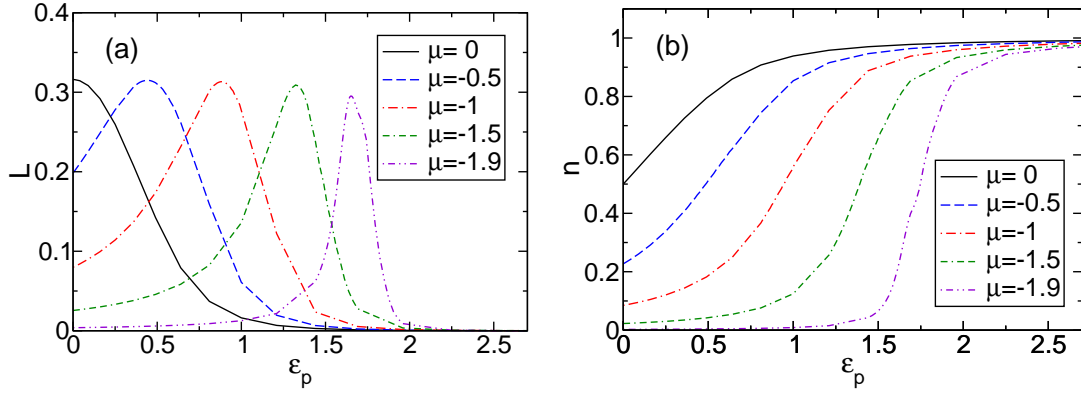


Figure 13. All results for $\Delta = 0$, $t = 1$, $t_d = 0.5$ and $\omega_0 = 1$. Kinetic coefficient L (a) and dot density n (b) as functions of ε_p for varying chemical potential μ .

now in the adiabatic regime. Owing to the values of the parameters μ and ω_0 , we have a situation where $\text{Im } \Sigma_{dd}(\omega) \neq 0$ in the whole relevant ω region and the spectral function is given by equation (29). According to the formula for $\text{Im } \Sigma_{dd}(\omega)$, equation (24), the cases $\varepsilon_p = 0.1$ [panel (c)] and $\varepsilon_p \lesssim \varepsilon_p^c$ [panel (d)] show the predominance of the first term. The shift of spectral weight to negative ω becomes apparent for $\varepsilon_p = 0.6$, indicating the influence of the EP interaction. The spectral function for $\varepsilon_p \gtrsim \varepsilon_p^c$ [panel (e)] and $\varepsilon_p = 1.6$ make evident the suppression of the first-term contribution and the multi-phonon structure according to the second term in equation (24). The maxima of the spectral function are situated near $\omega = \tilde{\eta}$. Then again the sudden decrease of L at ε_p^c may be understood from equation (54) by the sudden change of $A_{dd}(0)$ at ε_p^c .

Figure 13, for $\omega_0 = 1$, shows the maxima of L and the particle density on the dot, n , for $\mu \leq 0$, whereas the dot spectral function is given in figure 14 for $\mu = -1.9$ only. Different to the case $t_d = 1$, now a maximum in L is observed which, as μ decreases, moves to larger values of the EP coupling, simply because the effective dot level has to be lowered by a larger ε_p to match the Fermi level. For $\varepsilon_p = 1.2$ [panel (a)], the spectrum lies in the interval $[-W - \mu, W - \mu] \simeq [-0.1, 3.9]$, where the first term of equation (24) contributes, with the apparent influence of EP coupling. For larger ε_p , the spectrum is shifted towards $\omega < 0$. The point where the maximum in A_{dd} at $\tilde{\eta} = -\mu - \Delta - \varepsilon_p$ passes zero corresponds to the maximum of L . For $\mu = -1.9$, intervals with $\text{Im } \Sigma(\omega) = 0$ exist, namely for $\omega \in (-(s+1)\omega_0, -s\omega_0 - 0.1)$, where $s \geq 1$. The corresponding peak of an undamped state may be seen in panels (c) and (d) between $\omega = -2$ and $\omega = -1$.

Finally, we monitor for the wide-band case the transition induced by an increasing dot level Δ (see figure 15 at small ($\omega_0 = 0.1$, left-hand column) and intermediate-to-large ($\omega_0 = 1$, right-hand column) phonon frequencies). In both cases $\text{Im } \Sigma_{dd}(\omega) \neq 0$ for all ω . As discussed above, for $\Delta \neq 0$, $\tilde{\eta} = \Delta - \mu - \varepsilon_p \gamma(2 - \gamma)$, and the maximum in A_{dd} occurs near $\omega = \Delta - \varepsilon_p \gamma(2 - \gamma)$. In particular, for $\Delta = -2$ (panel (d)) the spectrum consists practically only of one peak at about $\Delta - \varepsilon_p$ with relatively small

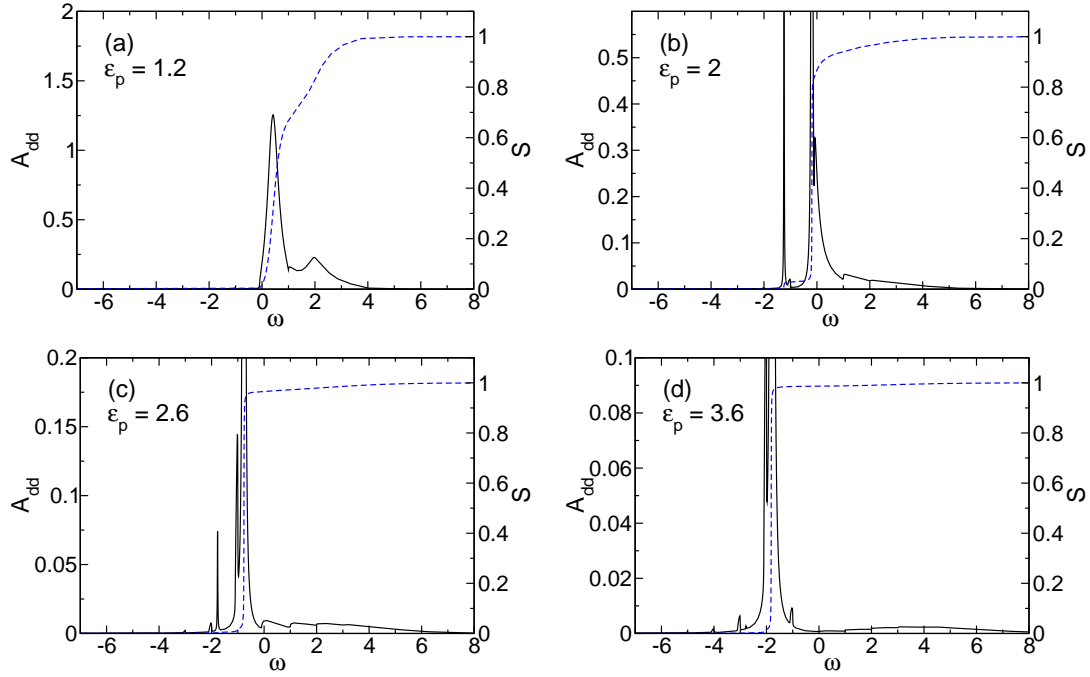


Figure 14. (Colour online) Dot spectral function for $\Delta = 0$, $t = 1$, $t_d = 0.5$, $\omega_0 = 1$, $\mu = -1.9$ and varying ε_p .

linewidth. Hence only a weakly damped localised state of the current carrier on the dot exists, having an energy lowering equal to ε_p . The transition from a localised to a delocalised carrier is accompanied by the shift of spectral weight to larger frequencies and the influence of the first term in equation (24) is recovered. The change of $A_{dd}(0)$ with Δ leads to the maximum observed for L at $\Delta - \varepsilon_p = 0$ in panel (b).

4. Summary

In this work, we have presented an approach to transport through a vibrating molecular quantum dot, which extends a previously developed description for the many-polaron problem. The virtue of this approach lies in an incomplete variational Lang-Firsov transformation in which the degree of the transformation is determined self-consistently. In this way, our approach can describe polaronic effects on transport away from the strong-coupling anti-adiabatic regime. Descriptions based on a full Lang-Firsov transformed Hamiltonian are, in contrast, restricted to this limit.

With our approach we studied the molecular quantum dot in different regimes, from weak to strong coupling and small to large phonon frequency. The dot spectral-functions, calculated within a second-order equation of motion approach, allow for a detailed analysis of the dynamical properties of the quantum dot in dependence of the model parameters. Our results show that the use of an incomplete Lang-Firsov transformation is essential to capture the physics for all but very large phonon frequencies. In almost

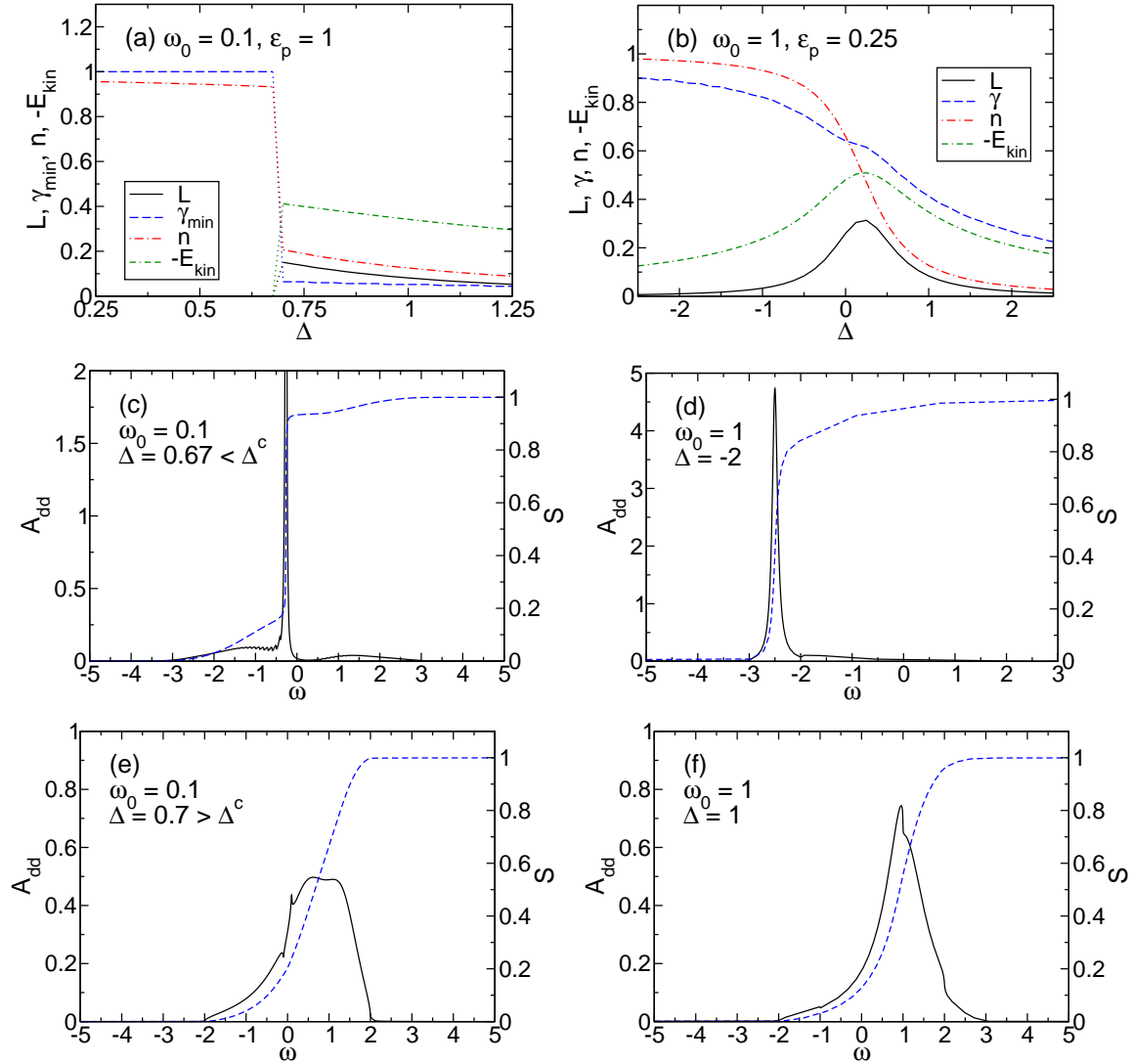


Figure 15. (Colour online) Left column: L , γ_{\min} , n and E_{kin} as functions of Δ for $t = 1$, $t_d = 0.5$, $\omega_0 = 0.1$, $\varepsilon_p = 1$ and $\mu = 0$ [(panel (a))]. At $\Delta^c \approx 0.68$ a crossover takes place. Spectral functions for Δ below [panel (c)] and above Δ^c [panel (e)]. Right column: L , γ_{\min} , n and E_{kin} as functions of Δ for $t_d = 0.5$, $\omega_0 = 1$, $\varepsilon_p = 0.25$ and $\mu = 0$ [panel (b)]. Panels (d) and (f) give the spectral functions $A_{dd}(\omega)$ and integrated spectral weight $S(\omega)$ for various Δ .

any cases, the optimal parameter γ differs significantly from unity.

The present study is open for extension in several important directions. On the one hand, extension to finite voltage bias is necessary. Since our approach is developed in the Green function formalism, this extension, e.g. using Keldysh techniques, is possible and will be addressed next. On the other hand, our approach correctly captures the physics for a large range of possible parameters, but even with an incomplete Lang-Firsov transformation one encounters problems at very small phonon frequency.

In conclusion, the presented work carries over important concepts and ideas well known from polaron physics, especially the crucial modification of the Lang-Firsov

transformation, to the study of vibrating molecular quantum dots.

Acknowledgements

This work was supported by Academy of Sciences Czech Republic (J.L.), Deutsche Forschungsgemeinschaft through SFB 652 (A.A.), and U.S. Department of Energy (A.R.B.). H.F. acknowledges the hospitality at the Institute of Physics ASCR and Los Alamos National Laboratory. The authors would like to thank M. Hohenadler and G. Wellein for valuable discussions.

References

- Alexandrov A S & Bratkovsky A M 2003 *Phys. Rev. B* **67**, 235312.
- Alvermann A & Fehske H 2008 *Phys. Rev. B* **77**, 045125.
- Alvermann A, Fehske H & Trugman S A 2008 *Phys. Rev. B* **78**, 165106.
- Bronold F X, Alvermann A & Fehske H 2004 *Philos. Mag.* **84**, 673.
- Bronold F X & Fehske H 2002 *Phys. Rev. B* **66**, 073102.
- Bruevich V L B & Tyablikov S V 1962 *The Green Function Method in Statistical Mechanics* North-Holland Amsterdam.
- Chen J, Read M A, Rawlett A M & Tour J M 1990 *Science* **286**, 1550.
- Cuniberti G, Fagas G & Richter K, eds 2005 *Introducing Molecular Electronics* Vol. 739 of *Lecture Notes in Physics* Springer Berlin Heidelberg.
- Emin D 1986 *Phys. Rev. B* **33**, 3973.
- Fehske H, Ihle D, Loos J, Trapper U & Büttner H 1994 *Z. Phys. B* **94**, 91.
- Fehske H, Loos J & Wellein G 1997 *Z. Phys. B* **104**, 619.
- Fehske H & Trugman S A 2007 in A. S Alexandrov, ed., ‘Polarons in Advanced Materials’ Vol. 103 of *Springer Series in Material Sciences* Canopus/Springer Publishing Dordrecht pp. 393–461.
- Fehske H, Wellein G, Loos J & Bishop A R 2008 *Phys. Rev. B* **77**, 085117.
- Flensberg K 2003 *Phys. Rev. B* **68**, 205323.
- Galperin M, Ratner M A & Nitzan A 2007 *J. Phys. Condens. Matter* **19**, 103201.
- Gerlach B & Löwen H 1991 *Rev. Mod. Phys.* **63**, 63.
- Hohenadler M & Fehske H 2007 *J. Phys.: Condens. Matter* **19**, 255210.
- Holstein T 1959a *Ann. Phys. (N.Y.)* **8**, 325.
- Holstein T 1959b *Ann. Phys. (N.Y.)* **8**, 343.
- Kadanoff L P & Baym G 1962 *Quantum Statistical Mechanics* Benjamin/Cumming Publishing Company Reading, Massachusetts.
- Koch T 2009 Transport durch molekulare quanten-punkte: polaronische effekte diploma thesis Universität Greifswald.
- Kubatkin S, Danilov A, Hjort M, Cornil J, Bredas J L, Stuhr-Hansen N, Hedegard P & Bjornholm T 2003 *Nature* **425**, 698.
- Lang I G & Firsov Y A 1962 *Zh. Eksp. Teor. Fiz.* **43**, 1843.
- Loos J, Hohenadler M, Alvermann A & Fehske H 2006 *J. Phys. Condens. Matter* **18**, 7299.
- Loos J, Hohenadler M, Alvermann A & Fehske H 2007 *J. Phys. Condens. Matter* **19**, 2362.
- Loos J, Hohenadler M & Fehske H 2006 *J. Phys. Condens. Matter* **18**, 2453.
- Meir Y & Wingreen N S 1992 *Phys. Rev. Lett.* **68**, 2512.
- Mishchenko A S, Nagaosa N, Alvermann A, Fehske H, Filippis G, Cataudella V & Sushkov O P 2009 *Phys. Rev. B*.
- Mitra A, Aleiner I & Mills A J 2004 *Phys. Rev. B* **69**, 245302.
- Nuñez Regueiro M D, Cornaglia P S, Usaj G & Balseiro C A 2007 *Phys. Rev. B* **76**, 075425.

Park H 2007 *Nature Mat.* **6**, 330.

Park J, Pasupathy A N, Goldsmith J L, Chang C, Yaish Y, Petta J R, Rinkoski M, Sethna J P, na H D A, McEuen P L & Ralph D C 2002 *Nature* **417**, 722.

Reichert J, Ochs R, Beckmann D, Weber H B, Mayor M & v. L"ohneysen H 2002 *Phys. Rev. Lett.* **88**, 176804.

Rickayzen G 1981 *Green's Functions and Condensed Matter* Academic Press.

Schnakenberg J 1966 *Z. Phys.* **190**, 209.

Takei S, Kim Y B & Mitra A 2005 *Phys. Rev. B* **72**, 075337.

Wellein G & Fehske H 1998 *Phys. Rev. B* **58**, 6208.

Zazunov A & Martin T 2007 *Phys. Rev. B* **76**, 033417.

Zubarev D N 1971 *Nonequilibrium Statistical Thermodynamics* Nauka Moscow.